

Large Margin Discriminative Loss for Classification

Hai-Vy Nguyen ^{*†‡}, Fabrice Gamboa[†], Sixin Zhang[‡], Reda Chhaibi [§], Serge Gratton[‡], and Thierry Giaccone^{*}

Abstract. In this paper, we introduce a novel discriminative loss function with large margin in the context of *Deep Learning*. This loss boosts the discriminative power of neural networks, represented by *intra-class compactness* and *inter-class separability*. On the one hand, the class compactness is ensured by close distance of samples of the same class to each other. On the other hand, the inter-class separability is boosted by a margin loss that ensures the minimum distance of each class to its closest boundary. All the terms in our loss have an explicit meaning, giving a direct view of the obtained feature space. We analyze mathematically the relation between compactness and margin term, giving a guideline about the impact of the hyper-parameters on the learned features. Moreover, we also analyze properties of the gradient of the loss with respect to the parameters of the neural network. Based on this, we design a strategy called *partial momentum updating* that enjoys simultaneously *stability* and *consistency* in training. Furthermore, we provide theoretical insights explaining why our method can avoid trivial solutions that do not improve the generalization capability of the model. Besides, we also investigate generalization errors to have better theoretical insights. The experiments show promising results of our method.

Key words. Deep Learning, Neural Network, Loss Function, Large Margin Loss, Center Loss

MSC codes. 68T01,68T07, 62-08

1. Introduction. The standard approach to train a neural network for classification is based on a *softmax* loss. This loss consists of a softmax layer and the cross-entropy divergence. However, one of the main drawbacks of this loss is that it generally only helps the network to produce separable, but not sufficiently discriminative features [16, 11]. In many problems, the intra-class variation is very large, meaning that the samples in each class are very diverse. But at the same time, the inter-class separability is small. That is, there exists some samples originating from different classes but they are very similar. This makes the prediction much more difficult. For instance, in the problem of classifying road surfaces, we need to determine whether the surface is dry, wet or watered. The boundary between dry and wet or wet and watered can be unclear. As a result, the separability between the classes is very small. At the same time, within each class, the road surface can be composed of different types of materials such as asphalt, concrete, etc. This leads to high intra-class variation.

Therefore, to achieve optimal generalization capability, a good machine learning algorithm in general, and a neural network in particular, should learn to produce features with high intra-class compactness and high inter-class separability [25].

To reach this goal, we introduce in this paper a novel loss function on the features of the penultimate layer (right before the softmax layer) in addition to the softmax loss. As this loss

^{*}Ampere Software Technology (hai-vy.nguyen@ampere.cars, thierry.giaccone@ampere.cars.)

[†]Institut de mathématiques de Toulouse (fabrice.gamboa@math.univ-toulouse.fr)

[‡]Institut de Recherche en Informatique de Toulouse (sixin.zhang@irit.fr, serge.gratton@toulouse-inp.fr.)

[§]Laboratoire Jean Alexandre Dieudonné, Université Côte d'Azur, (reda.chhaibi@univ-cotedazur.fr).

applies only on this penultimate layer, it can be used generically on any neural network model, for an end-to-end training, based on any gradient-based optimization method. Our new loss function is the combination of two terms: a *hinge center loss* and a *margin loss*. The hinge center loss shall appear in Eq. (4.4) and ensures compactness. By minimizing this loss, the intra-class compactness of features is maximized. Notice that a center loss has been used in some previous works (e.g. [23]). This latter loss directly minimizes the distance of each feature to its class centroid. This could lead the model to a mode collapse [20], where the model learns to project all the samples of each class to a sole point. To avoid this undesirable situation, one needs to add a quite complex penalty term and to be careful in the training process. On the contrary, in our method, inspired by the work of [3], we opt for a hinge center loss, which only pushes the distance of each point to its centroid to be smaller than a predefined positive term δ_v . This allows us to avoid the collapse phenomenon. On the other hand, the margin loss shall appear in Eq. (4.5) and boosts the *class margin*. Here, the *class margin* of a given class is defined as its distance from the decision boundary. For this purpose, we first derive an exact analytical formula for the decision boundaries (see Section 4.1). Based on this, we also provide an analytical formula for the class margin and so we are able to maximize this margin. In addition, we derive some mathematical insights on the relation between the hyperparameters both of the hinge center loss and the margin loss, providing a lower bound for the class margin.

Ideal features should have their maximal intra-class distance smaller than their minimal inter-class distance [11], especially for classification problems where the samples in each class possess high variability while samples from different classes are quite similar. Enforcing the model to produce these “ideal features”, it can learn more accurately the representative characteristics of each class (so that intra-class distance is small). At the same time, it focuses more on the characteristics that makes the difference between classes (so that the minimal inter-class distance is larger than the maximal intra-class distance). This boosts the discriminative power of the learned features. By deriving analytically both the relation between the compactness term and the margin term of our loss and the hyper-parameters, we can explicitly enforce the model to produce ideal features.

Besides, we directly compute the gradients of this loss with respect to the parameters of the neural network. This provides some insights about gradients. Some properties of the gradient leads to difficulty in updating the parameters. Based on this, we design a strategy, called *partial momentum* to overcome this drawback. This gives simultaneously, *stability* and *consistency* in the training process.

Our contributions can be summarized as follows:

- The loss function provided here enables to model both class compactness and margin simultaneously in a softmax model using an explicit formula available in Eq. (4.3).
- We provide theoretical insights for a better understanding of feature learning in softmax models. More precisely, we provide theoretical insights explaining why our method allows for avoiding trivial solutions that do not improve the generalization capability of the model. We also derive theoretical results in the form of test error bounds also known as generalization bounds. These are stated as Theorems 5.2 and 5.3.
- We conduct experiments on standard datasets. According to the quantitative results,

our loss function systematically boosts the test accuracy compared to softmax loss, proving that our insights are on point. The qualitative results lead us to the same conclusion.

- Thanks to our experiments, we find that by only boosting the discriminative power of the penultimate layer of a neural network, the features of the intermediate layers also become more discriminative. This is further supported by a theoretical result in the form of our Theorem 6.3.

Our paper is organized as follows. Section 2 compares our method with related works. Section 3 recalls mathematically the framework of softmax models. In Section 4, we discuss about theoretical decision boundaries and then present our method. Section 5 provides theoretical insights on generalization errors. As our loss is applied only on the penultimate layer of a model, we also derive theoretical insights about the impact of our loss on intermediate layers in Sections 6. Finally, we conduct experiments in Section 7. Our code is available on Github at the repository [margin-compact-loss](#).

2. Related works. The work [23] proposes a center loss applied in parallel to the standard softmax loss. This loss encourages the direct minimization of the distance between each point and the centroid of the corresponding class (in feature space). As discussed in [20], this could lead to *feature collapse*, where all the samples of each class collapse to a sole point. Therefore, one needs to add a penalty term and to be very careful in the training process to guarantee sensitivity of the model with respect to the inputs. Here, we avoid the problem by using a *hinge center loss*, inspired by the work of [3]. This only enforces the distance from centroid to be smaller than a certain predefined distance. Furthermore, center loss in [23] only explicitly encourages intra-class compactness and the inter-class margins are not taken into account. Hence, there is no guarantee about the margin in [23].

The benefits of large-margin in the context of deep learning is pointed out in [12], [11] and [4]. In these works the authors ignore the bias terms of the softmax layer, and consequently the margin can be expressed only via angles between vectors. This is referred to as *angular margin*. In contrast, our method makes no change in the softmax layer and we calculate explicitly the margin based directly on the Euclidean distance. Moreover, their methods only encourage inter-class margin while the intra-class compactness is not explicitly considered. As discussed in the introduction, in scenarios where intra-variance class is large, intra-class compactness is necessary.

In the more recent work [25], intra-class compactness and inter-class separability are both considered. However, the method of [25] completely ignores the magnitude of class prototypes to come up with the final loss. Moreover, this method only maximize the distance between classes (in some sense), without considering the decision boundaries. Indeed, even with good inter-class separability, poorly placed decision boundaries can reduce its effectiveness. If the decision boundary is too close to a class, new examples may easily cross it, leading to poor classification.

In the work of [5], the class margin from the decision boundaries is considered. This method is based on the same ideas behind the classical SVM [6] in the sense that it imposes a minimum value for the margin of each class to the decision boundaries. Indeed, this paper proposes to boost the margins for the different layers of a neural network using a first-order

approximation. In contrast, our method models the margin directly on the feature space of the penultimate layer. Our method therefore provides an exact formula for both the decision boundaries and the class margins from these boundaries. Moreover, the method proposed in [5] does not consider the intra-class compactness contrarily to ours.

The work in [19], also based on a margin approach, proposes to apply the multi-class SVM in the context of Deep Learning. However, this method is based on a *one-versus-rest* approach, i.e. one needs to separately train C classifiers for C classes. This makes the training much more heavy in the context of Deep Learning. In contrast, our method proposes a loss that consider all the classes simultaneously. Moreover, the intra-compactness is totally ignored therein.

The idea of learning features based on within-class and between-class similarities was exploited in the so-called *circle loss* [17]. The high-level idea of this method consists in 2 ingredients: class-level labels and pair-wise labels. With class-level labels, one pushes each sample to be close to its true class prototype, and to be far from others. Using pair-wise labels, one pushes samples such that cosine-similarity of features in the same class is larger than that of features coming from different classes, with certain margin. While the idea is intuitive, how this approach impacts the *classification decision boundaries* is not clear. For instance, even if the classes are well separated in the feature space but the classification boundaries are too close to one class, a good classification is not guaranteed. This is in contrast to our method where the decision boundaries are taken into account.

The idea of using similarity between samples for feature learning is also very popular in *contrastive learning*. The idea is to maximize similarities between *positive samples* and to minimize those between *negative samples* [1, 15, 9, 22].

3. Preliminaries and framework. Let us consider a classification problem with C classes ($C \geq 2$). The input space is denoted by \mathcal{X} , which can be a space of images, time series or vectors. The neural network (backbone) transforms an input into a fixed-dimension vector. Formally we model the network by a function: $f_\theta : \mathcal{X} \mapsto \mathcal{F} \subseteq \mathbb{R}^d$, where θ is the set of parameters of the neural network, d is the dimension of the so-called *feature space* \mathcal{F} . That is, \mathcal{F} is the representation space induced from \mathcal{X} by the transformation f_θ . Given an input $x \in \mathcal{X}$, set $q = q(x) = f_\theta(x)$. In order to perform a classification task, q is then passed through a softmax layer consisting of an affine (linear) transformation (Eq. (3.1)) and a *softmax* function (Eq. (3.2)). Expressed in formal equations, we have

$$(3.1) \quad z = Wq + b, \quad W \in \mathbb{R}^{C \times d} \text{ and } b \in \mathbb{R}^C,$$

$$(3.2) \quad \sigma(z)_i = \frac{e^{z_i}}{\sum_{j=1}^C e^{z_j}}.$$

Here, for $i = 1, \dots, C$, z_i is the i^{th} component of column-vector z . The predicted class is then the class with maximum value for $\sigma(z)$, i.e. $\hat{y} = \arg \max_i \sigma(z)_i$.

Remark 3.1. We note that $\arg \max_i \sigma(z)_i = \arg \max_i z_i$. So that, $\hat{y} = \arg \max_i z_i$.

In the standard approach, to train the neural network to predict maximal score for the right class, the softmax loss is used. This loss is written as

$$(3.3) \quad \mathcal{L}_S = -\frac{1}{|\mathcal{B}|} \sum_{(x,y) \in \mathcal{B}} \log \sigma(Wf_\theta(x) + b)_y .$$

Here, \mathcal{B} is the current mini-batch, x being a training example associated with its ground-truth label $y \in \{1, 2, \dots, C\}$. By minimizing this loss function w.r.t. θ and (W, b) , the model learns to assign maximal score to the right class.

4. Large margin discriminative loss.

4.1. Decision boundaries and the drawback of softmax loss. Consider the pair of classes $\{i, j\}$. We have:

$$(4.1) \quad z_i - z_j = (Wq + b)_i - (Wq + b)_j = \langle W_i - W_j, q \rangle + (b_i - b_j).$$

Here, $z = \begin{pmatrix} z_1 \\ \vdots \\ z_C \end{pmatrix}$ and $W = \begin{pmatrix} W_1^T \\ \vdots \\ W_C^T \end{pmatrix}$ with for $j = 1, \dots, C$, $W_j \in \mathbb{R}^d$. Set

$$(4.2) \quad \mathcal{P}_{ij} = \{q \in \mathcal{F} , \langle W_i - W_j, q \rangle + (b_i - b_j) = 0\} .$$

Notice that $\{q \in \mathcal{F} : z_i(q) > z_j(q)\}$ and $\{q \in \mathcal{F} : z_i(q) < z_j(q)\}$ are the two half-spaces separated by \mathcal{P}_{ij} . Hence, the decision boundary for the pair $\{i, j\}$ is the hyperplane \mathcal{P}_{ij} , and for $q \in \mathcal{P}_{ij}$, the scores assigned to the classes i and j are the same. Using Eq. (3.3), for an input of class i , we see that the softmax loss pushes z_i to be larger than all other z_j 's ($j \neq i$), i.e., $\langle W_i - W_j, q \rangle + (b_i - b_j) > 0$. Hence, the softmax loss enforces the features to be in the right side w.r.t. decision hyper-planes. Notice further that this loss has a contraction effect. Indeed, inputs of the same class lead to probability vectors close to each other and close to an extremal point of Δ^C , the simplex in \mathbb{R}^C of probability measures¹. Furthermore, we may observe that the softmax function is translation invariant by the vector $\varepsilon \mathbb{1}$, whose components are all equal to $\varepsilon \in \mathbb{R}$. Hence, even for two inputs of the same class that output exactly the same probability vectors, it may happen that their corresponding logit vectors z 's are very far from each other. Consequently, the feature vectors q 's of the same class are not explicitly encouraged to be close to each other. If somehow this is the case, then it is an intrinsic property of a well-designed neural network, and not the consequence of using softmax loss. As discussed in the introduction section, intra-class compactness is important for a better generalization capacity of the model. Hence, it is desirable to have a loss that explicitly encourages this property.

4.2. Proposed Loss Function. To have a better classification, we rely on the following two factors: intra-class compactness and inter-class separability. To obtain these properties, we work in the feature space \mathcal{F} . In many classification problems, the intra-class variance is

¹Formally, $\Delta^C = \{(p_1, \dots, p_C) \in \mathbb{R}^C \mid \sum_{i=1}^C p_i = 1, p_i \geq 0 \forall i\}$

very large. So, by forcing the model to map various samples of the same class in a compact representation, the model learns the representative features of each class and ignores irrelevant details. Moreover, it may happen that samples in different classes are very similar. This leads to misclassification. Hence, we also aim to learn a representation having large margins between classes. In this way, the model learns the characteristics that differentiate between classes. Hence, it classifies better the samples. To achieve all these objectives, we propose the following loss function:

$$(4.3) \quad \mathcal{L} = \alpha \cdot \mathcal{L}_{\text{compact}} + \beta \cdot \mathcal{L}_{\text{margin}} + \gamma_{\text{reg}} \cdot \mathcal{L}_{\text{reg}} .$$

Here, $\mathcal{L}_{\text{compact}}$, $\mathcal{L}_{\text{margin}}$ and \mathcal{L}_{reg} force for class compactness, inter-class separability and regularization, respectively. We now discuss in detail these three terms. Let us consider the current mini-batch \mathcal{B} . Let $\mathcal{C}_{\mathcal{B}}$ be the set of classes in \mathcal{B} and $\mathcal{C}_c^{\mathcal{B}}$ be the examples of class c in \mathcal{B} . To ensure intra-class compactness, we use the discriminative loss proposed in [3]. Note that in the latter article, this loss is used in the different context of image segmentation. This loss is written

$$(4.4) \quad \mathcal{L}_{\text{compact}} = \frac{1}{|\mathcal{C}_{\mathcal{B}}|} \times \sum_{c \in \mathcal{C}_{\mathcal{B}}} \frac{1}{|\mathcal{C}_c^{\mathcal{B}}|} \sum_{q \in \mathcal{C}_c^{\mathcal{B}}} [\|m_c - q\| - \delta_v]_+^2 .$$

Here, $\|\cdot\|$ is the Euclidean norm, $[q]_+ = \max(0, q)$ and m_c is the centroid of the class c . This function is zero when $\|m_c - q\| < \delta_v$. Hence, this function enforces that the distance of each point to its centroid is smaller than δ_v . Notice that this function only pushes the distance to be smaller than δ_v and not to be zero. Hence, we avoid the phenomenon of mode collapse.

To have a better inter-class separability, we build a loss function enforcing large margin between classes and at the same time taking into account the decision boundaries. A naive strategy would be to maximize distance of each sample to all the decision boundaries (see for example [5]). However, this is very costly and not really necessary. Instead, we propose to maximize the distance of each centroids to the decision boundaries. Indeed, we will give in Proposition 4.2 a lower bound for the class margins. The margin loss is defined as follows,

$$(4.5) \quad \mathcal{L}_{\text{margin}} = \frac{1}{|\mathcal{C}_{\mathcal{B}}|} \times \sum_{c \in \mathcal{C}_{\mathcal{B}}} \max_{i \neq c} [\delta_d + d(m_c, \mathcal{P}_{ci}) \text{ sign}((m_c)_i - (m_c)_c)]_+ .$$

This function is inspired by the work of [5]. Intuitively, when the centroid m_c is on the right side of the decision boundary, $(m_c)_i - (m_c)_c < 0$. Hence, in this case we minimize $[\delta_d - d(m_c, \mathcal{P}_{ci})]_+$ and consequently $d(m_c, \mathcal{P}_{ci})$ is encouraged to be larger than δ_d . In contrast, if m_c is on the wrong side of the decision boundary, then we minimize $[\delta_d + d(m_c, \mathcal{P}_{ci})]_+$. This enforces m_c to pass to the right side. Hence, this loss is only deactivated if the centroid is on the right side w.r.t all the decision boundaries and its distance to the decision boundaries are larger than δ_d . Moreover, notice that we opt for the aggregation operation $\max_{i \neq c}$ instead of $\text{mean}_{i \neq c}$. Indeed, it may happen that some pairs of class are easier to separate than others. With *mean* aggregation, loss can be minimized by focusing only on easy pairs and ignoring

difficult pairs. In contrast, with aggregation max, we enforce the neural networks to focus on difficult pairs. As such, it can learn more useful features to increase discriminative power. Notice that the distance of m_c to the hyperplane \mathcal{P}_{ci} , the decision boundary of class pair (c, i) , can be computed explicitly as,

$$(4.6) \quad d(m_c, \mathcal{P}_{ci}) = \frac{|\langle W_c - W_i, m_c \rangle + (b_c - b_i)|}{\|W_c - W_i\|}.$$

Our loss function encourages each centroids to be far away from the decision boundaries. However, there are no guarantee that the decision boundaries lead to closed cells. The resulted centroids could be pushed far away. Hence, to address this problem, we add a regularization term as proposed in [3],

$$(4.7) \quad \mathcal{L}_{\text{reg}} = \frac{1}{|\mathcal{C}_{\mathcal{B}}|} \sum_{c \in \mathcal{C}_{\mathcal{B}}} \|m_c\|.$$

Note that this regularization term is optional, meaning that we can set $\gamma_{\text{reg}} = 0$.

4.3. Properties of intra-class compactness and inter-class separability. In this section, we investigate the properties of compactness and separability of the loss function. Furthermore, we discuss the impact of the hyper-parameters δ_v and δ_d . This gives us a guideline on the choice of these hyper-parameters.

Definition 4.1 (Class dispersion). We define the dispersion of a given class c as the maximal Euclidean distance between two samples in this class i.e. $\text{dispersion}(c) := \max_{p, q \in \mathcal{C}_c} \|p - q\|$.

Proposition 4.1. If $\mathcal{L}_{\text{compact}} = 0$, then the dispersion of all classes is at most $2\delta_v$.

Proof. See Appendix A.1. ■

This last proposition shows that the hinge center loss ensures the intra-compactness property of each class.

Definition 4.2 (Class margin). Let us define the margin of a given class c as the smallest Euclidean distance of samples in this class to its closest decision boundary, i.e.

$$\text{margin}(c) := \min_{q \in \mathcal{C}_c} \left(\min_{i \neq c} d(q, \mathcal{P}_{ci}) \right).$$

Proposition 4.2. Assume that $\mathcal{L}_{\text{compact}} = \mathcal{L}_{\text{margin}} = 0$. Then,

1. If $\delta_d > \delta_v$, then the margin of all classes is at least $\delta_d - \delta_v$.
2. If $\delta_d > 2\delta_v$, then the distances between any points in the same class are smaller than the distances between any points from different classes.

Proof. See Appendix A.2. ■

Hence, if we aim to obtain class margin at least ε , then we can set $\delta_d = \delta_v + \varepsilon$. Furthermore, this proposition provides a guideline for the choice of δ_v and δ_d . We are aiming for a representation with not only a large inter-class margin, but also one in which the distances

between points in the same class are smaller than the distances between points in different classes. This is particularly useful for problems where samples in each class are too diverse whereas samples from different classes are too similar. Indeed, by enforcing this property in the feature space, the model learns more useful representative characteristics of each class. So that, intra-class distance is small even for dissimilar samples of the same class. At the same time, the model focuses more on the characteristics that makes the difference between classes. In this way, even very similar samples but coming from different classes are better separated.

4.4. Partial momentum for centroids. Let us now consider a class c . To compute the centroid of this class, there are 2 straightforward ways:

- **Naive way.** Using all the sample of the considered class in the current mini-batch: $m_c^t := m_c^{\text{current}} = \frac{1}{|\mathcal{C}_c^{\mathcal{B}}|} \sum_{q \in \mathcal{C}_c^{\mathcal{B}}} q$.
- **Using momentum.** $m_c^t := m_c^{\text{momentum}} = \gamma \cdot m_c^{t-1} + (1 - \gamma) \cdot m_c^{\text{current}}$, where γ is chosen to be close to 1, such as 0.9.

One major advantage of using momentum is stability. Recall that in modern machine learning, very small mini-batches, as small as a size of 1, are now common to achieve speed-ups at the cost of noisy gradient steps. Thus it can happen that the centroid of each class fluctuates too much from one batch to another. In such case, we do not have a stable direction to that centroid. As $\mathcal{L}_{\text{compact}}$ aims to push each point to its corresponding centroid, the optimization becomes less effective. Hence, the use of momentum allows us to avoid this problem. However, using momentum makes the gradient much smaller when updating the model parameters. More precisely, we have following proposition:

Proposition 4.3. $\nabla_{\theta} \mathcal{L}_{\text{margin}}^{\text{moment}} = (1 - \gamma) \cdot \nabla_{\theta} \mathcal{L}_{\text{margin}}^{\text{naive}}$. Here, $\mathcal{L}_{\text{margin}}^{\text{naive}}$ and $\mathcal{L}_{\text{margin}}^{\text{moment}}$ are the margin losses computed using the centroids updated based on naive way and momentum way, respectively.

Proof. See Appendix B. ■

This proposition shows that using centroid with or without momentum gives the same gradient direction. Nevertheless, with momentum the very small shrinking scaling factor $1 - \gamma$ appears.

Further, this small gradient is multiplied by a small learning rate (typically in the range $[10^{-5}, 10^{-2}]$). So, on the one hand, the parameter updating in the momentum method is extremely small (or even get completely canceled out by the computer rounding limit or *machine epsilon*). On the other hand, as discussed previously, using momentum allows more stability. To overcome the gradient drawback but to conserve the stability benefit, we combine the naive and momentum ways. We come up with a strategy named *partial momentum*. This strategy uses momentum for the compactness loss and naive way for the margin loss, respectively. Doing so, we have stable centroids. So that, each point is pushed in a stable direction. But at the same time, the centroids are kept *consistent*. That is, the parameters of the neural network evolve along training with sufficiently large gradients.

4.5. To square the loss or not to square the loss. We can notice that each term under the sum operation in $\mathcal{L}_{\text{compact}}$ is squared, whereas this is not the case for $\mathcal{L}_{\text{margin}}$. Indeed, squared of each term leads to more relaxed loss than non-squared version. More formally, when the term under the sum operation of $\mathcal{L}_{\text{compact}}$ and $\mathcal{L}_{\text{margin}}$ is still activated, its general

form can be written as

$$f(u) = \begin{cases} \pm \|u - u_{\text{ref}}\| + b, & \text{if non-squared version} \\ (\pm \|u - u_{\text{ref}}\| + b)^2, & \text{if squared version} \end{cases}$$

where u_{ref} is the reference point. In the case of $\mathcal{L}_{\text{compact}}$, $\|u - u_{\text{ref}}\|$ is the distance from a generic point to its corresponding centroid denoted here by u_{ref} . In the case of $\mathcal{L}_{\text{margin}}$, $\|u - u_{\text{ref}}\|$ is the distance of a centroid to its projection on the closest boundary. For sake of simplicity, we ignore here the sign before $\|u - u_{\text{ref}}\|$ as here this does not matter. So, we have

$$\nabla_u f = \begin{cases} \frac{u - u_{\text{ref}}}{\|u - u_{\text{ref}}\|}, & \text{if non squared version} \\ 2(\|u - u_{\text{ref}}\| + b) \times \frac{u - u_{\text{ref}}}{\|u - u_{\text{ref}}\|}, & \text{if squared version} \end{cases},$$

which implies

$$\|\nabla_u f\| = \begin{cases} 1, & \text{if non squared version} \\ 2 \times \left| \|u - u_{\text{ref}}\| + b \right|, & \text{if squared version} \end{cases}.$$

Consider the regime where u approaches u_{ref} . If not squared, the gradient remains of constant magnitude as long as it is still activated. In contrast, if the term is squared, then, for states close to be deactivated, $\|u - u_{\text{ref}}\| + b$ is close to 0. Hence, the gradient is very small. Thus, the magnitude of the update direction for u becomes minimal when it is close to the deactivated state.

Following this discussion, on the one hand, squaring in $\mathcal{L}_{\text{compact}}$ gives a smoother and less stringent loss. For example, if there are very abnormal points, then this condition does not enforce completely the points to be in the hyper-sphere around their centroid. On the other hand, by not squaring for the margin loss, we enforce stronger conditions on the centroid until it attains the deactivated state. That is, its distance to the closest boundary is at least larger than δ_d . This is important as the position of each centroid impact the distribution of the whole class. This insight justifies our proposed loss functions.

4.6. Why the compactness loss or margin loss alone does not suffice. Recall that the Huygens Inertia Theorem decomposes total inertia into a sum of inter-class inertia and intra-class inertia. As such, as in the context of clustering for example, minimizing intra-class inertia is equivalent to maximizing inter-class inertia. Because of that, one may wrongly think that boosting only one of these inertias suffices. However, in the context of classification, and more generally feature learning, we train our model to produce relevant features and the initial cloud of features is not fixed. Let us thus discuss the respective effects of a compactness loss and a margin loss on the discriminative power of a neural network.

In order to boost class compactness, one can minimize the distance of each point to the corresponding class centroid. As presented in Section 2, this approach is proposed in [23] using a center loss. Boosting the class margin is proposed by [5]. However, we shall prove that applying only one of these two approaches can fail. Indeed, they can lead to trivial solutions that allow for enforcing class compactness or class margin but where the predictions of the model remain unchanged – and so does the generalization capability. In such cases, the

model is not encouraged to learn more discriminative features. This also suggests that the use of both compactness and margin is necessary. More formally, let us consider a softmax model \mathcal{N} that is defined as in Section 3. Denote the parameters of \mathcal{N} by Θ . We suppose that the layer prior to the feature space \mathcal{F} is a convolutional or fully-connected layer, that can be followed or not followed by the non-linearity *ReLU*. Let \mathcal{N}_Θ be the current neural network.

Proposition 4.4. *For $\alpha > 0$, there exists a map, depending on α , \mathcal{T}_α , such that $\tilde{\Theta} = \mathcal{T}_\alpha(\Theta)$ satisfies $\mathcal{N}_{\tilde{\Theta}}(x) = \mathcal{N}_\Theta(x)$ for all $x \in \mathcal{X}$. Furthermore,*

1. *If \mathcal{N}_Θ is such that $\min_c \text{margin}(c) = d_{\text{margin}} > 0$ (see Definition 4.2), then, for the new model $\mathcal{N}_{\tilde{\Theta}}$, $\min_c \text{margin}(c) = \alpha d_{\text{margin}}$.*
2. *If \mathcal{N}_Θ is such that $0 < \max_c \text{dispersion}(c) = d_{\text{dispersion}}$ (see Definition 4.1), then, for the new model $\mathcal{N}_{\tilde{\Theta}}$, $\max_c \text{dispersion}(c) = \alpha d_{\text{dispersion}}$.*
3. *$\mathcal{T}_\alpha(\Theta) - \Theta = (\alpha - 1)u$, where u is a vector depending only on Θ .*

Proof. See Appendix C. ■

Corollary 4.1. *$\forall \alpha_1, \alpha_2 > 1$, $\mathcal{T}_{\alpha_1}(\Theta) - \Theta$ and $\mathcal{T}_{1/\alpha_2}(\Theta) - \Theta$ are vectors of opposite directions.*

In particular, as α_1 or α_2 increase, the movement of parameters happens in opposite directions. That is, using this family of transformations, the class margin expansion and the class dispersion shrinkage cannot happen at the same time.

Suppose that we are given a network \mathcal{N}_Θ with certain class margin and dispersion – and that was trained with softmax loss for example. We note that the statements (1) and (2) in Proposition 4.4 hold for all $\alpha > 0$. This indicates that, by choosing $\alpha < 1$ or $\alpha > 1$, we can explicitly perform a transformation to obtain new parameters of \mathcal{N} that satisfy the constraints imposed by either center loss or margin loss alone, respectively, without changing the predictions of \mathcal{N} . That is, the model is not really encouraged to learn more discriminative features and the generalization of the model is not improved. However, Corollary 4.1 tells that we cannot both expand the class margin and shrink the class dispersion simultaneously. This is because Θ is moved in two exactly opposite directions. Thus, by maximizing the class margin and minimizing the class dispersion simultaneously, our loss guarantees that transformations along opposite directions cannot occur. That is, our loss can avoid a solution that do not improve the generalization error of the model.

Finally, we also note that by choosing $\alpha > 1$ (resp. $\alpha < 1$), \mathcal{T}_α expands (resp. shrinks) simultaneously the class margin and the class dispersion, without changing the model predictions. This suggests that, the performances of the model can be unchanged when scaling the two hyper-parameters δ_v and δ_d with a same factor $\alpha > 0$. Hence, when working with these two hyper-parameters, we can fix either δ_v or δ_d , and change only the other one. In our experiment, we fix δ_v , and test with different values for δ_d (see ablation study in Section 7.2.1).

5. Generalization error. In this section, we investigate the generalization error of our method. For this, we first recall the notion of margin loss introduced in [13].

Definition 5.1 (Margin loss function). For any $\rho > 0$, the ρ -margin loss is the function $L_\rho : \mathbb{R} \times \mathbb{R} \mapsto \mathbb{R}_+$ defined for all $y, y' \in \mathbb{R}$ by $L_\rho(y, y') = \Phi_\rho(y y')$ with,

$$(5.1) \quad \Phi_\rho(x) = \begin{cases} 1 & \text{if } x \leq 0. \\ 1 - x/\rho & \text{if } 0 \leq x \leq \rho. \\ 0 & \text{if } \rho \leq x. \end{cases}$$

Interpretation. Considering $y \in \{-1, +1\}$ as ground-truth label and $y' := h(x)$ as the decision function, correct predictions correspond to the points with $yh(x) > 0$. Therefore, this loss penalizes the points with wrong decision (i.e. $yh(x) < 0$) or with correct decision but with *confidence level* $yh(x) < \rho$. Hence, ρ can be regarded as a confidence parameter. If we have no demand about confidence level in the decision, we can set $\rho = 0$. In this case, the margin loss becomes the function $1_{\{h(x)y < 0\}}$, which penalizes the wrong predictions ($yh(x) < 0$).

We will set our main theoretical results. The next subsections give and discuss non asymptotic bound theoretical risks.

5.1. Pairwise classification generalization error. We note that multi-classification can be seen as separate classifications in pairs. In other words, each class has to be separated from the other classes. Therefore, for the sake of simplicity, we study the pairwise classification at a theoretical level to produce generalization bounds. To that endeavor, we assume here that the input (X, Y) ($X \in \mathcal{X}$ and $Y \in \{-1, 1\}$), consists in a binary mixture and we aim to quantify the binary classification error of our method. The next theorem relates this error to the empirical one obtained on the training sample. Let S denote the sample consisting in $N > 0$ independent copies of (X, Y) . Recall that \mathcal{F} denotes the feature space and let $\mathcal{M}(\mathcal{X}, \mathcal{F})$ be the set of all measurable functions from \mathcal{X} to \mathcal{F} . Let $R > 0$ and $m_1, m_2 \in \mathcal{F}$ such that $\|m_i\| \leq R$, ($i = 1, 2$). Given $r > 0$, our oracle bounds involve the following functional set

$$\mathcal{G}_1 = \left\{ f \in \mathcal{M}(\mathcal{X}, \mathcal{F}) : \sup_{x \in \mathcal{X}} \min(\|f(x) - m_1\|, \|f(x) - m_2\|) \leq r \right\}.$$

Our first theorem writes,

Theorem 5.2. Define $R(h) := \mathbb{E}[\mathbb{1}_{\{Yh(X) < 0\}}]$ and $\widehat{R}_{S, \rho}(h) := \frac{1}{N} \sum_{i=1}^N \Phi_\rho(y_i h(x_i))$, for $h \in \mathcal{M}(\mathcal{X}, \mathcal{F})$. They are respectively the generalization error and the empirical error. Then

1. Given a fixed mapping $f \in \mathcal{G}_1$ and $\Gamma > 0$, let $H_f = \left\{ \langle f(\cdot), w \rangle + b : \left\| \begin{pmatrix} w \\ b \end{pmatrix} \right\| \leq \Gamma \right\}$. For any $\delta > 0$, with probability at least $1 - \delta$, the following inequality holds,

$$(5.2) \quad R(h) \leq \widehat{R}_{S, \rho}(h) + \frac{2\Gamma \sqrt{(r+R)^2 + 1}}{\rho \sqrt{N}} + 3\sqrt{\frac{\log \frac{2}{\delta}}{2N}}, \quad (h \in H_f).$$

2. Let $H_1 = \bigcup_{f \in \mathcal{G}_1} H_f$. For any $\delta > 0$, with probability at least $1 - \delta$ we have,

$$(5.3) \quad R(h) \leq \widehat{R}_{S, \rho}(h) + \frac{2\Gamma \sqrt{(r+R)^2 + 1}}{\rho} + 3\sqrt{\frac{\log \frac{2}{\delta}}{2N}}, \quad (h \in H_1).$$

Proof. See Appendix D.1. ■

Remarks. First of all, it is natural to work with the functional class \mathcal{G}_1 , since the loss function (4.6) imposes the mapping of the input to the balls of each class in the feature space. Secondly, assuming that $\|m_1\|$ and $\|m_2\|$ are both bounded by R is a reasonable assumption in view of the regularization term (4.7). In addition, to bound the theoretical loss, we use the empirical margin loss instead of our own. However, it is obvious that minimizing our loss leads to minimize the empirical margin loss. In fact, using our loss tends to separate the two classes and increase margins as shown in Proposition 4.2. Lastly, notice the difference between the two upper bounds provided in the last theorem. The first is local because f is fixed, whereas the second is valid for all f . This explains the degradation in the second term of Eq. (5.3).

5.2. Generalization error of mapping each point to a hyper-sphere. In the above subsection, we have considered the pairwise classification. Furthermore, in our method, the loss contains a compactness component that enforces each point to be mapped in a hypersphere centered on the centroid of its class (in feature space). By imposing the model to satisfy this constraint on the training set, we expect to have the same property on the test set. *Is this a reasonable objective?* To answer this question, we now fix a particular class and quantify the mapping error. That is, the probability that a point is projected outside the correct hyper-sphere. The following theorem provides an empirical upper bound for this probability. Here, S denote the sample consisting in $N > 0$ independent copies of X . Let $R, r, \Lambda > 0$, our oracle bound involves the following functional set

$$H_2 = \left\{ r^2 - \|f(\cdot) - m\|^2 : \|m\| \leq R, f \in \mathcal{M}(\mathcal{X}, \mathcal{F}), \sup_{x \in \mathcal{X}} \|f(x)\| \leq \Lambda \right\}.$$

Our second theorem writes,

Theorem 5.3. *For any $\delta > 0$, with probability at least $1 - \delta$ over the draw of an i.i.d. sample S of size N , for any $h \in H_2$, we have,*

$$(5.4) \quad \mathbb{P}(h(X) < 0) \leq \widehat{R}'_{S,\rho}(h) + \frac{2}{\rho}(\Lambda^2 + 2R\Lambda + \frac{R^2}{\sqrt{N}}) + 3\sqrt{\frac{\log \frac{2}{\delta}}{2N}}.$$

Here, $\widehat{R}'_{S,\rho}(h) = \frac{1}{N} \sum_{i=1}^N \Phi_\rho(h(x_i))$ is the empirical margin loss on S .

Proof. See Appendix D.2. ■

Remarks. Notice that if an input x is mapped into a point inside the hyper-sphere (in the feature space), then $h(x) > 0$. Hence, $\mathbb{P}(h(X) < 0)$ measures the average error, i.e. examples whose mapping lies outside the hyper-sphere.

Notice also that on one hand, when $\rho = 0$, $\widehat{R}'_{S,\rho}(h)$ only penalizes training examples whose mapping is outside the hyper-sphere ($h(x) < 0$). On the other hand, when $\rho > 0$, it additionally penalizes examples mapped inside the hyper-sphere but having a margin from the hyper-sphere boundary less than ρ . We also remark that the upper bound (5.4) gets smaller as the number of training examples N gets larger. Obviously, this is expected, as with larger N , the training examples cover better the underlying input distribution. Hence, the model tends to well behave on the test set, if it is well trained (i.e. small empirical loss on training set).

6. Impact on the features of intermediate layers. Our loss is only applied on the features of the penultimate layer. So, an important question is: *does that really impacts the features of intermediate layers?* In this section, we provide theoretical insights about this question.

Let $X \in \mathcal{X}$ and $Y \in \mathcal{Y}$ denote the random variables (r.v.), modeling respectively the input and the label. Let \mathcal{D}_X and \mathcal{D}_Y be the distributions of X and Y , respectively. In the feature space \mathcal{F} , the feature r.v. Q can be written as $Q := f_\theta(X)$. That is, the distribution \mathcal{D}_Q of Q is induced from \mathcal{D}_X by f_θ (\mathcal{D}_Q is called *induced distribution*). Given $y \in \mathcal{Y}$, let $\mathcal{D}_{Q|y}$ be the induced distribution from the conditional input distribution $\mathcal{D}(X|Y = y)$. We recall that our loss aims to enforce features of different classes to be contained in different hyper-spheres. Hence, in some sense, it pushes away $\mathcal{D}_{Q|y}$ from $\mathcal{D}_{Q|y'}$, for any $(y \neq y') \in \mathcal{Y}^2$. In this way, the features of different classes can be more separable.

Now, let us consider an arbitrary intermediate layer l before the penultimate layer. In an analogous way, let Q_l be the r.v. of this layer and let $\mathcal{D}_{Q_l|y}$ denote the conditional induced distributions of this layer. Now, the question is: *For all $(y \neq y') \in \mathcal{Y}^2$, does our loss make $\mathcal{D}_{Q_l|y}$ more separated from $\mathcal{D}_{Q_l|y'}$?* In order to measure the divergence between distributions, we first recall some definitions.

Definition 6.1 (Kullback–Leibler divergence). Let \mathcal{D}_1 and \mathcal{D}_2 be probability measures on a measurable space Ω . The Kullback–Leibler divergence (KL divergence) between \mathcal{D}_1 and \mathcal{D}_2 is defined as $D_{KL}(\mathcal{D}_1 || \mathcal{D}_2) = \int_{\omega \in \Omega} \log \left(\frac{d\mathcal{D}_1}{d\mathcal{D}_2}(\omega) \right) \mathcal{D}_1(d\omega)$, and $+\infty$ if the Radon-Nikodym derivative $\frac{d\mathcal{D}_1}{d\mathcal{D}_2}$ does not exist.

We note that D_{KL} is not symmetric. To overcome such drawbacks, we can use the Jensen-Shannon divergence with the following definition.

Definition 6.2 (Jensen–Shannon divergence (JSD)). Let \mathcal{D}_1 and \mathcal{D}_2 be probability measures on a measurable space Ω . The Jensen–Shannon divergence (JSD) between \mathcal{D}_1 and \mathcal{D}_2 is defined as $D_{JS}(\mathcal{D}_1 || \mathcal{D}_2) = \frac{1}{2}D_{KL}(\mathcal{D}_1 || \bar{\mathcal{D}}) + \frac{1}{2}D_{KL}(\mathcal{D}_2 || \bar{\mathcal{D}})$, where $\bar{\mathcal{D}} = \frac{1}{2}(\mathcal{D}_1 + \mathcal{D}_2)$ is a mixture distribution of \mathcal{D}_1 and \mathcal{D}_2 .

Now, let us consider a trained model with our method. Recall that the compactness loss encourages the features in \mathcal{F} of each class y to be contained in a hyper-sphere of radius δ_v and centered at m_y , denoted by $\mathcal{S}(m_y, \delta_v)$. Thus, it is natural to make the following margin assumption

(H) There exists a τ ($1/2 \leq \tau \leq 1$) such that for all $y \in \mathcal{Y}$, we have $\mathcal{D}_{Q|y}(\mathcal{S}(m_y, \delta_v)) := \mathbb{P}(Q \in \mathcal{S}(m_y, \delta_v) | Y = y) \geq \tau$.

Under this assumption, the probability that each point is projected in the right hyper-sphere is at least $\tau \geq 1/2$. This is a reasonable assumption if the model is well trained. Under the assumption (H), we have the following theorem.

Theorem 6.3. Let $(y \neq y') \in \mathcal{Y}^2$. For any intermediate layer l before the penultimate layer, we have

$$(6.1) \quad D_{JS}(\mathcal{D}_{Q_l|y} || \mathcal{D}_{Q_l|y'}) \geq (2\tau - 1)^2/2 .$$

Proof. See Appendix E. ■

This theorem gives a lower bound for the JSD between the conditional feature distributions of intermediate layers. If the model is well trained, τ gets larger, so does $D_{JS}(\mathcal{D}_{Q^l|y} || \mathcal{D}_{Q^l|y'})$. That is, in the intermediate layers, features of different classes become more separated from each other. The intuition behind this is rather simple. Indeed, let us argue using contradiction reasoning in an informal manner. Suppose for example that $\mathcal{D}_{Q^l|y}$ is very similar to $\mathcal{D}_{Q^l|y'}$ and that they share a large part of their supports. Then, the features of this layer are propagated until the feature space \mathcal{F} by the same mapping – which is the set of layers between layer l and the penultimate layer. Hence, the two conditional distributions $\mathcal{D}_{Q|y}$ and $\mathcal{D}_{Q|y'}$ in \mathcal{F} should be also similar. This contradicts the condition imposed by our loss, where features of different classes should be contained in distinct hyper-spheres. Hence, $\mathcal{D}_{Q^l|y}$ should be distinct from $\mathcal{D}_{Q^l|y'}$ so that these constraints on the penultimate layer are satisfied. Theorem 6.3 formalizes this idea. Indeed, this matches the results observed in our experiments (see Section 7.4).

7. Experiments. In this section, we first perform experiments on 2 standard datasets: CIFAR10 [10] and The Street View House Numbers (SVHN) [14]. CIFAR10 contains 50000 training images and 10000 test images of 10 classes (including vehicles and animals). SVHN has 73257 training images and 26032 for testing. For these two datasets, we use ResNet18 [7] as backbone, followed by some fully connected layers prior to softmax layer. Then, we test our method on a large-scale dataset RSCD [24] with nearly one million training images (detail about this dataset is in Section 7.5). For this dataset, we test on two different models EfficientNet-b0 [18] and MobileNetV3 [8]. Thus, by testing on different models with different sizes and structures (ResNet18, EfficientNet-b0 and MobileNetV3), we get a better view on the performance of our method. Note that the softmax loss is applied at the output as it helps to produce separable features (as discussed in Section 4.1). In addition to the softmax loss, our loss is applied in the feature of penultimate layer to boost the discriminative power of the features. All the details for conducting our experiments can be found in Appendix F.

7.1. Ablation study. In this part, without further mention, we fix batch size equal to 128. We also fix $\gamma_{\text{reg}} = 10^{-3}$ for regularization term in our loss. We also fix momentum factor for centroid updating to $\gamma = 0.99$ (see Section 4.4 for definition of γ).

7.2. Impact of compactness and margin component. First, we fix $\delta_v = 0.5$ and $\delta_d = 1.5$. Then, we experiment on three cases: $\alpha = 0, \beta = 1$ (no compact loss, only margin loss), $\alpha = 1, \beta = 0$ (no margin loss, only compact loss) and $\alpha = 1, \beta = 1$ (both compact and margin losses). For each of the two datasets CIFAR10 and SVHN, we train models using only a fraction of the training set. Then, the model is evaluated on the full test set. The results of test accuracy at different fraction of training set are shown in Fig. 1. We see that using both compact and margin losses leads to the best results on both datasets. We also remark that using only compact loss ($\alpha = 1, \beta = 0$) seems to perform better than using only margin loss ($\alpha = 0, \beta = 1$). This reinforces the theoretical insights presented in Section 4.1, in which we show that softmax loss encourages separable features but provides no guarantee for class compactness. So, the compact loss is likely to be more important than the margin loss. However, the use of margin loss in addition to the compact one is still better.

7.2.1. Impact of δ_v and δ_d . As discussed in Section 4.6, changing both δ_v and δ_d by a same factor α can lead to models with a same performance. Thus, we fix $\delta_v = 0.5$ and test with

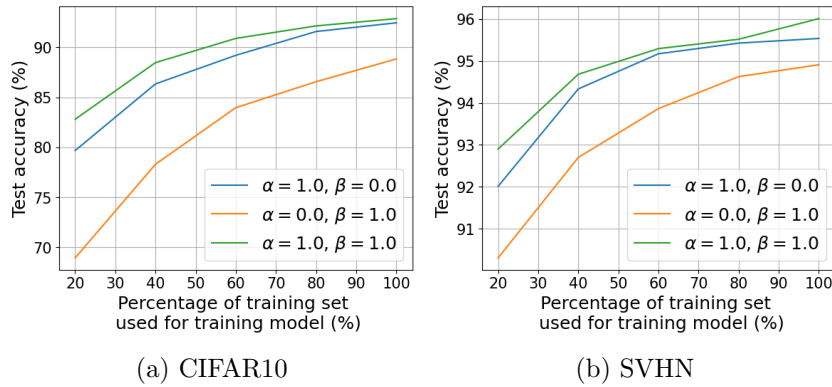


Figure 1: Ablation study compact and margin loss on datasets CIFAR10 and SVHN. Fixing $\delta_v = 0.5$, $\delta_d = 1.5$, we experimented with and without compact/margin loss.

different values for δ_d . The results are shown in Fig. 2 and Table 1. We see that when δ_d is too small ($\delta_d = \delta_v = 0.5$), the model performs not well at different percentages of the training set. When increasing the value of δ_d , the model performance seems to be improved. In many cases, $\delta_d = 6.0$ performs the best. Moreover, in many cases, increasing δ_d to be larger than 6.0 either harms the model performance or leads to very marginal performance improvements (see Table 1). For instance, $\delta_d = 8.0$ performs worse than $\delta_d = 6.0$. This might be explained by the fact that when δ_d is too large (compared to δ_v), the model is encouraged to focus more on the features that make the difference between classes (so that different classes are far away from each other in the feature space), and it could ignore some important features that are useful for generalization on new examples at inference times.

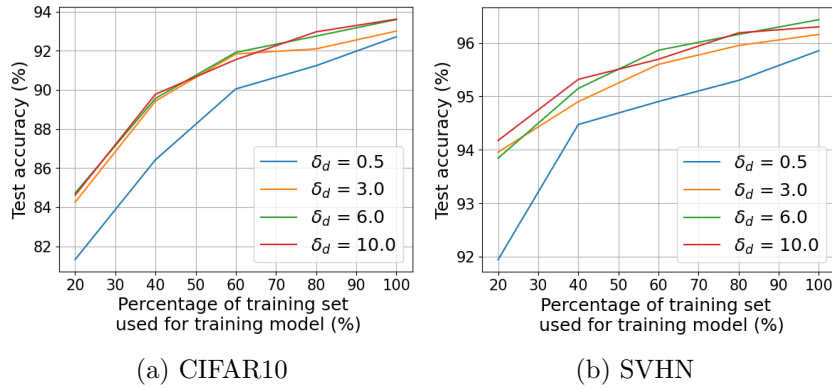


Figure 2: Ablation study δ_v and δ_d . Fixing $\delta_v = 0.5$, we experimented with different values of δ_d . For a best visualization, we show here only 4 values of δ_d but more values can be found in Table 1.

Table 1: Accuracy (%) on full test set of CIFAR10 and SVHN. Models are trained using different fractions (%) of training set and different values of δ_d , by fixing $\delta_v = 0.5$ in our loss.

Dataset	train. percent (%)	0.5	1.0	1.5	2.0	3.0	4.0	6.0	8.0	10.0
CIFAR10	20	81.330	82.370	82.800	84.280	84.260	84.440	84.730	85.140	84.620
	40	86.430	87.700	88.460	88.750	89.430	89.080	89.570	89.540	89.780
	60	90.050	90.240	90.880	90.710	91.840	91.530	91.920	91.720	91.550
	80	91.240	91.310	92.130	92.460	92.100	92.640	92.750	92.810	92.970
	100	92.720	92.650	92.860	92.910	93.010	93.490	93.600	93.440	93.620
SVHN	20	91.941	92.471	92.901	93.685	93.954	93.996	93.842	93.931	94.173
	40	94.472	94.342	94.683	94.607	94.899	95.294	95.148	95.160	95.317
	60	94.902	95.091	95.294	95.429	95.598	95.640	95.863	95.621	95.694
	80	95.298	95.517	95.517	95.847	95.951	95.963	96.159	96.182	96.189
	100	95.855	95.709	96.009	96.120	96.159	96.316	96.435	96.331	96.301

7.2.2. Impact of momentum. Now, we evaluate the impact of momentum for updating the centroids (as discussed in Section 4.4). For this, we experiment with 3 strategies: (i) *no momentum*, meaning that we do not use momentum for centroid updating in both compact and margin loss; (ii) *both momentum*, meaning that we use momentum for centroid updating in both compact and margin loss and (iii) *partial momentum* (see Section 4.4). Similarly to the previous experiments, we use different fractions of the training set for training. Based on the results of the previous section, we fix $\delta_v = 0.5$ and $\delta_d = 6.0$ for both datasets. The results of test accuracy on the full test sets of CIFAR10 and SVHN are shown in Fig. 3 and Table 2. A first remark is that *both momentum* performs much worse than the 2 other strategies. This reinforces our theoretical insights which point out that using the momentum in the margin loss creates a shrinkage in gradient magnitude, making it more difficult to optimize the centroids. Another remark is that at a sufficient large percentage of training set (from 70%), *partial momentum* performs slightly better than *no momentum*. In contrast, at smaller fraction, *no momentum* seems to perform slightly better. This might be explained by the fact that, at smaller fractions, we have less data and we use sufficiently large batch size (128). So, the centroids might stay quite stable from one batch to another. Hence, the momentum might be less important in such cases.

Table 2: Ablation study of momentum: accuracy on test set of CIFAR10 and SVHN at different fractions (%) of training set, by fixing $\delta_v = 0.5$ and $\delta_d = 6.0$.

Dataset	train. percent (%)	20	40	60	80	100
CIFAR10	no momentum	85.220	89.800	91.790	92.350	93.430
	both momentum	73.580	82.260	87.870	91.050	92.690
	partial momentum	84.730	89.570	91.920	92.750	93.600
SVHN	no momentum	94.026	95.298	95.908	96.089	96.143
	both momentum	91.771	94.456	95.432	95.954	96.097
	partial momentum	93.842	95.148	95.863	96.159	96.435

7.3. Comparing our method with softmax loss on CIFAR10 and SVHN. We now compare our method with softmax loss to see how our loss helps to boost the discriminative power

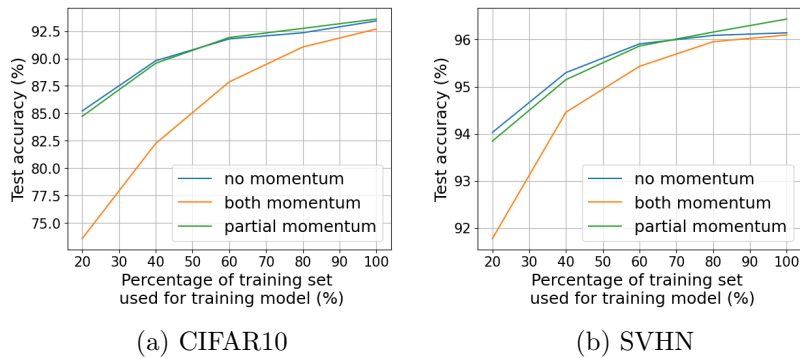


Figure 3: Ablation study of momentum. We fix $\delta_v = 0.5$, $\delta_d = 6.0$.

of the models. For this objective, we use two datasets CIFAR10 and SVHN. For our loss, we fix $\delta_v = 0.5$ and $\delta_d = 6.0$ without any further tuning. We first qualitatively evaluate how our loss function helps to boost class compactness and inter-class separability compared to the softmax loss. To this end, we first train a model on the training set of CIFAR10 (resp. of SVHN). Next, we compute the features of the test set of CIFAR10 (resp. of SVHN). Finally, we use the technique of t-SNE [21] for visualizing feature in a 2D space. The results are shown in Fig. 4. Each color represents a class. We see that by using softmax loss (Fig. 4a and 4c), the classes are not so well separated in the feature space. On the contrary, our method boost significantly the inter-class separation (Fig.4b and 4d). Note that the models do not see the test set during training. Thus, these results confirm that our method really helps to boost discriminative power on new sample.

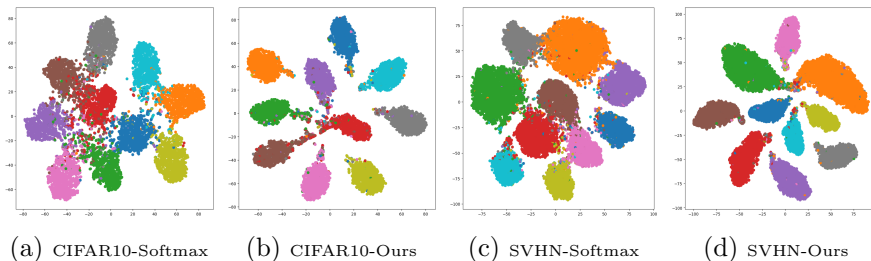


Figure 4: t-SNE on test images of CIFAR10 and SVHN in the feature space after training with softmax loss and our loss function. Note that the models do not see the test set during training.

Next, we evaluate how our loss function helps the model generalize better on the test set by comparing test accuracy. For each of the two datasets CIFAR10 and SVHN, we use only a sample fraction of the training set for training models. Then we evaluate the model on the full test set, comparing softmax loss to ours. The results are shown in Table 3 and

Fig. 5. We find that at different percentages of the training set, on both datasets, our method consistently performs significantly better than softmax loss in terms of test accuracy. Moreover, for CIFAR10, with only 60% of the learning set, our methods already outperform the softmax loss, which uses the full training set. For SVHN, remarkably, with only 40% of the training set, our method already gives the same test accuracy as the softmax model using the full training set. These results prove that our loss function helps the model to have a better generalization ability with less training data.

Table 3: Accuracy (%) on the full test sets of CIFAR10 and SVHN at different training percentages of training set.

Dataset	Percentage of training data (%)	20	40	60	80	100
CIFAR10	softmax	77.920	85.270	88.970	90.180	91.170
	ours	84.730	89.570	91.920	92.750	93.600
SVHN	softmax	90.573	93.246	94.095	94.387	95.013
	ours	93.842	95.184	95.863	96.159	96.435

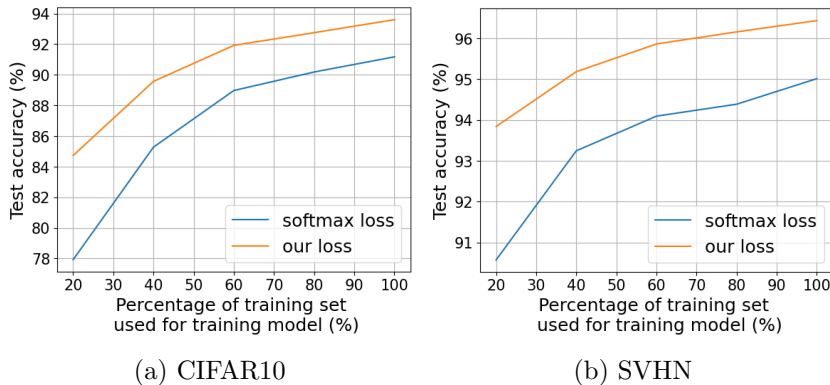


Figure 5: Test accuracy of CIFAR10 and SVHN after training using only a certain fraction of training set with softmax loss and our loss.

7.4. Impact of our loss function on intermediate layers. In the experiments above, we use ResNet18 [7] as backbone, followed by some fully connected layers prior to softmax layer. Recall that our loss function is applied on the feature of the penultimate layer (right before softmax layer). Hence, it is interesting to see the impact of this loss function on the model. Indeed, the results shown in Figure 4 are the features of penultimate layer. It could be argued that our loss function only impacts the last fully connected layers to provide discriminating features, and does not really impact the backbone. Section 6 already gives us theoretical insights. In this section, to answer this question experimentally, we perform the same t-SNE technique for the intermediate layers of the backbone. ResNet18 includes 4 main blocs, each gives outputs of dimension $H_i \times W_i \times C_i$, ($i = 1, \dots, 4$). H_i and W_i are spatial dimensions (and

so depend on the input dimension). C_i is the number of channels of the bloc i (independent of the input dimension). For each input, we first perform a *Global Average Pooling* over the spatial dimensions to obtain a feature vector of dimension C_i (for each bloc i). Then t-SNE is performed as before. The results for CIFAR10 and SVHN are shown in Figures 6 and 7.

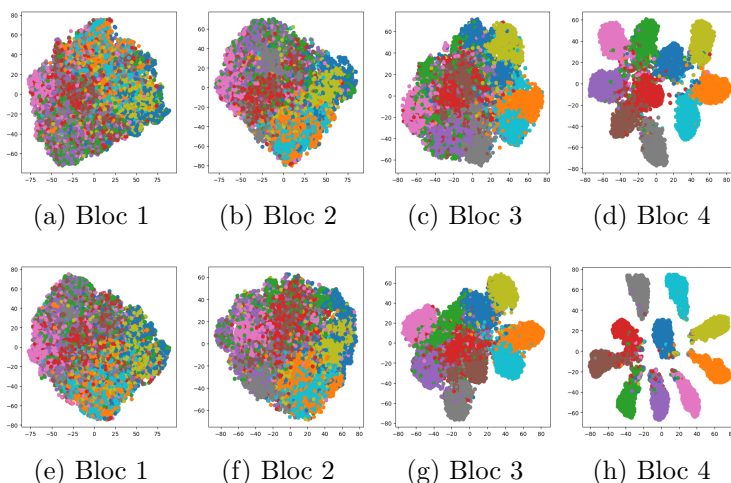


Figure 6: t-SNE of CIFAR10 test images for different intermediate layers with softmax loss and our loss function. Top row: softmax loss. Bottom row: our loss. Note that the models do not see the test set during training.

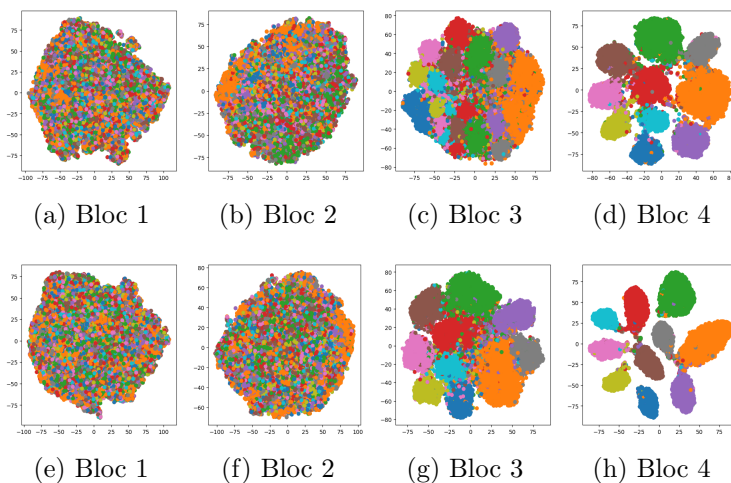


Figure 7: t-SNE of SVHN test images for different intermediate layers with softmax loss and our loss function. Top row: softmax loss. Bottom row: our loss. Note that the models do not see the test set during training.

For the two datasets, we observe that there is no distinctive clusters in the first two blocs. This is expected as these are shallow layers, and no semantic feature is really captured. However, from the bloc 3, our loss function seems to help the model to produce more distinctive clusters compared to softmax loss (Fig. 6g vs Fig. 6c for CIFAR10 and Fig. 7g vs Fig. 7c for SVHN). This effect is well observed for the bloc 4 for both datasets (Fig. 6h vs Fig. 6d for CIFAR10 and Fig. 7h vs Fig. 7d for SVHN). This implies that our loss function not only impacts the feature of the penultimate layer, but really helps the model to learn more discriminative features at the intermediate levels. This reinforces our theoretical insights in Section 6. In conclusion, our loss function is powerful in the classification task by neural networks.

7.5. Application on a large scale dataset for road surface classification. In this section, we apply our loss function in a problem of road surface classification. We use a large scale dataset named *Road Surface Classification Dataset* (RSCD) [24]. This dataset contains nearly one million training images, 20 thousands validation images and nearly 50 thousands test images. In total, there are 27 classes in this dataset, that are labeled based on material, friction and unevenness of the road surface. As this large-scale dataset is collected on various road conditions, the intra-class variance is very high, as discussed in the original paper [24]. Therefore, it is interesting to test our method.

Based on the results in Section 7.2.2, we know that the strategy *both momentum* gives results much worse than strategies *partial momentum* and *no momentum*. So, we apply only these two last strategies. For *partial momentum* strategy, we test with different momentum values. We use model *EfficientNet-b0* [18], which is used in [24]. Besides, we also test our method on model *MobileNetV3* [8]. We note that EfficientNet-b0 is approximately two times larger than MobileNetV3 in terms of FLOPS, meaning that EfficientNet-b0 is two times more time-demanding than MobileNetV3. Thus, testing on two models with different structures and scales gives us a better view of our method. Results are shown in Table 4.

First of all, we observe the performance of models trained with softmax loss on MobileNetV3 and EfficientNet-b0. Although MobileNetV3 costs twice as much in FLOPs as EfficientNet-b0, its test accuracy is increased by only about 0.3% (compared to MobileNetV3). This shows that improving the test accuracy on this dataset is challenging. Analyzing the performance on EfficientNet-b0 using center loss, we observe that the center loss helps to improve slightly the test accuracy. Nevertheless, this improvement is not really significant. In contrast, our method helps to improve the test accuracy more significantly on this large-scale dataset on both models. Moreover, using larger momentum for updating the class centroids (0.9 and 0.99 in our case) helps to improve the test accuracy, compared to smaller momentum (0.5 or no momentum in this case). This is aligned with our discussion in Section 4.4, where we argue that momentum helps to have a better stability.

Finally, we note that MobileNetV3 trained with our loss (with large momentums 0.9 and 0.99) already gives better performance than EfficientNet-b0 trained with the standard softmax loss. Knowing that EfficientNet-b0 is two times larger than MobileNetV3, these results are impressive. All these observations confirm once again that our method is useful for improving the generalization capability of model.

8. Conclusion. In this paper, we introduce a loss function for classification problems using softmax models with the purpose of boosting performance. This loss is model-agnostic as it is

Table 4: Accuracy on test set of RSCD.

Model	Loss	Momentum	Test accuracy (%)
MobileNetV3	softmax	No	91.63
	ours	0 (no momentum)	91.93
	ours	0.5	91.957
	ours	0.9	92.19
	ours	0.99	92.07
EfficientNet-b0	softmax	No	91.92
	center loss center loss [24]	No	92.05
	ours	0 (no momentum)	92.19
	ours	0.5	92.27
	ours	0.9	92.49
	ours	0.99	92.47

applied directly in the feature space of the penultimate layer. Its effect is to generically boost the compactness and inter-class margins for better classification.

We also give insights on our loss function for better understanding our method. The qualitative evaluations using t-SNE clearly show that our loss encourages more discriminative features. This is not only the case for the penultimate layer, but also for the intermediate layers. The numerical results once again confirm efficacy of our method. Indeed, using only a small part of training set with our loss function already gives the same test accuracy as training on the full training set with the softmax loss. In the light of our investigations, the loss proposed here can be a plug-and-play tool to improve the performance of any classification task using softmax models.

REFERENCES

- [1] T. CHEN, S. KORNBLITH, M. NOROUZI, AND G. HINTON, *A simple framework for contrastive learning of visual representations*, in International conference on machine learning, PMLR, 2020, pp. 1597–1607.
- [2] T. M. COVER AND J. A. THOMAS, *Elements of Information Theory 2nd Edition (Wiley Series in Telecommunications and Signal Processing)*, Wiley-Interscience, July 2006.
- [3] B. DE BRABANDERE, D. NEVEN, AND L. VAN GOOL, *Semantic instance segmentation with a discriminative loss function*, arXiv preprint arXiv:1708.02551, (2017).
- [4] J. DENG, J. GUO, N. XUE, AND S. ZAFEIRIOU, *Arcface: Additive angular margin loss for deep face recognition*, in Proceedings of the IEEE/CVF conference on computer vision and pattern recognition, 2019, pp. 4690–4699.
- [5] G. ELSAYED, D. KRISHNAN, H. MOBAHI, K. REGAN, AND S. BENGIO, *Large margin deep networks for classification*, Advances in neural information processing systems, 31 (2018).
- [6] S. R. GUNN ET AL., *Support vector machines for classification and regression*, ISIS technical report, 14 (1998), pp. 5–16.
- [7] K. HE, X. ZHANG, S. REN, AND J. SUN, *Deep residual learning for image recognition*, in Proceedings of the IEEE conference on computer vision and pattern recognition, 2016, pp. 770–778.
- [8] A. HOWARD, M. SANDLER, G. CHU, L.-C. CHEN, B. CHEN, M. TAN, W. WANG, Y. ZHU, R. PANG, V. VASUDEVAN, ET AL., *Searching for mobilenetv3*, in Proceedings of the IEEE/CVF international conference on computer vision, 2019, pp. 1314–1324.
- [9] P. KHOSLA, P. TETERWAK, C. WANG, A. SARNA, Y. TIAN, P. ISOLA, A. MASCHINOT, C. LIU, AND D. KRISHNAN, *Supervised contrastive learning*, Advances in neural information processing systems,

- 33 (2020), pp. 18661–18673.
- [10] A. KRIZHEVSKY, V. NAIR, AND G. HINTON, *Learning multiple layers of features from tiny images*, Technical Report, (2009), <http://www.cs.toronto.edu/~kriz/cifar.html>.
 - [11] W. LIU, Y. WEN, Z. YU, M. LI, B. RAJ, AND L. SONG, *Sphereface: Deep hypersphere embedding for face recognition*, in Proceedings of the IEEE conference on computer vision and pattern recognition, 2017, pp. 212–220.
 - [12] W. LIU, Y. WEN, Z. YU, AND M. YANG, *Large-margin softmax loss for convolutional neural networks*, arXiv preprint arXiv:1612.02295, (2016).
 - [13] M. MOHRI, *Foundations of machine learning*, Adaptive computation and machine learning series, MIT press, 2nd edition ed., 2018.
 - [14] Y. NETZER, T. WANG, A. COATES, A. BISSACCO, B. WU, A. Y. NG, ET AL., *Reading digits in natural images with unsupervised feature learning*, in NIPS workshop on deep learning and unsupervised feature learning, vol. 2011, Granada, 2011, p. 4.
 - [15] A. V. D. OORD, Y. LI, AND O. VINYALS, *Representation learning with contrastive predictive coding*, arXiv preprint arXiv:1807.03748, (2018).
 - [16] S. SUN, W. CHEN, L. WANG, X. LIU, AND T.-Y. LIU, *On the depth of deep neural networks: A theoretical view*, in Proceedings of the AAAI Conference on Artificial Intelligence, vol. 30, 2016.
 - [17] Y. SUN, C. CHENG, Y. ZHANG, C. ZHANG, L. ZHENG, Z. WANG, AND Y. WEI, *Circle loss: A unified perspective of pair similarity optimization*, in Proceedings of the IEEE/CVF conference on computer vision and pattern recognition, 2020, pp. 6398–6407.
 - [18] M. TAN AND Q. LE, *Efficientnet: Rethinking model scaling for convolutional neural networks*, in International conference on machine learning, PMLR, 2019, pp. 6105–6114.
 - [19] Y. TANG, *Deep learning using support vector machines*, CoRR, abs/1306.0239, 2 (2013).
 - [20] J. VAN AMERSFOORT, L. SMITH, Y. W. TEH, AND Y. GAL, *Uncertainty estimation using a single deep deterministic neural network*, in International conference on machine learning, PMLR, 2020, pp. 9690–9700.
 - [21] L. VAN DER MAATEN AND G. HINTON, *Visualizing data using t-sne.*, Journal of machine learning research, 9 (2008).
 - [22] F. WANG AND H. LIU, *Understanding the behaviour of contrastive loss*, in Proceedings of the IEEE/CVF conference on computer vision and pattern recognition, 2021, pp. 2495–2504.
 - [23] Y. WEN, K. ZHANG, Z. LI, AND Y. QIAO, *A discriminative feature learning approach for deep face recognition*, in Computer Vision–ECCV 2016: 14th European Conference, Amsterdam, The Netherlands, October 11–14, 2016, Proceedings, Part VII 14, Springer, 2016, pp. 499–515.
 - [24] T. ZHAO, J. HE, J. LV, D. MIN, AND Y. WEI, *A comprehensive implementation of road surface classification for vehicle driving assistance: Dataset, models, and deployment*, IEEE Transactions on Intelligent Transportation Systems, (2023).
 - [25] X. ZHOU, X. LIU, D. ZHAI, J. JIANG, X. GAO, AND X. JI, *Learning towards the largest margins*, arXiv preprint arXiv:2206.11589, (2022).

Appendix A. Proofs of intra-class compactness and inter-class separability.

A.1. Proof of Proposition 4.1.

Proof. Let q_1 and q_2 be 2 arbitrary points in any class c . By triangle inequality, we have: $\|q_1 - q_2\| \leq \|q_1 - m_c\| + \|m_c - q_2\| \leq \delta_v + \delta_v = 2\delta_v$. ■

A.2. Proof of Proposition 4.2. Proof of Proposition 4.2.1

Proof. Consider an arbitrary class c . Let p be a point in this class and let q be any point on the hyperplane \mathcal{P}_{ci} for any $i \neq c$. Then, by triangle inequality, we have:

$$\|m_c - q\| \leq \|m_c - p\| + \|p - q\|.$$

As $d(m_c, \mathcal{P}_{ci}) \geq \delta_d$, we have $\|m_c - q\| \geq \delta_d, \forall q \in \mathcal{P}_{ci}$. At the same time, we also have $\|m_c - p\| \leq \delta_v$. Consequently, we obtain:

$$\delta_d \leq \|m_c - q\| \leq \|m_c - p\| + \|p - q\| \leq \delta_v + \|p - q\|.$$

Hence, $\|p - q\| \geq \delta_d - \delta_v, \forall q \in \mathcal{P}_{ci}$. So, by definition, $d(p, \mathcal{P}_{ci}) \geq \delta_d - \delta_v$. This holds $\forall p \in \mathcal{C}_c$ and $\forall i \neq c$. Hence, $\text{margin}(c) = \min_{p \in \mathcal{C}_c} (\min_{i \neq c} d(p, \mathcal{P}_{ci})) \geq \delta_d - \delta_v$. As we choose an arbitrary class c , this holds for all classes. The proposition is proved.

Proof of Proposition 4.2.2

Proof. Let q_1 and q_2 be 2 arbitrary points in any class same c . By Proposition 4.1, we have: $\|q_1 - q_2\| \leq 2\delta_v$. Now, let p and q by 2 arbitrary points in any two different classes i and j , respectively. It suffices to show that $\|p - q\| > 2\delta_v$ with $\delta_d > 2\delta_v$. Again, by triangle inequality, we have:

$$\|m_i - m_j\| \leq \|m_i - p\| + \|p - m_j\| \leq \|m_i - p\| + (\|p - q\| + \|q - m_j\|).$$

So, $\|p - q\| \geq \|m_i - m_j\| - (\|m_i - p\| + \|q - m_j\|) \geq \|m_i - m_j\| - 2\delta_v$. Now, let us consider $\|m_i - m_j\|$. By Cauchy-Schwartz inequality, we have:

$$\left| \langle m_i - m_j, \frac{W_i - W_j}{\|W_i - W_j\|} \rangle \right| \leq \|m_i - m_j\| \cdot \frac{\|W_i - W_j\|}{\|W_i - W_j\|} = \|m_i - m_j\|.$$

Hence,

$$\begin{aligned} \|m_i - m_j\| &\geq \left| \frac{\langle W_i - W_j, m_i \rangle}{\|W_i - W_j\|} - \frac{\langle W_i - W_j, m_j \rangle}{\|W_i - W_j\|} \right| \\ &= \left| \frac{\langle W_i - W_j, m_i \rangle + (b_i - b_j)}{\|W_i - W_j\|} - \frac{\langle W_i - W_j, m_j \rangle + (b_i - b_j)}{\|W_i - W_j\|} \right| \end{aligned}$$

As m_i and m_j are on 2 different sides of the hyperplane \mathcal{P}_{ij} (which is the decision boundary), $\langle W_i - W_j, m_i \rangle + (b_i - b_j)$ is of opposite sign of $\langle W_i - W_j, m_j \rangle + (b_i - b_j)$. Hence,

$$\begin{aligned} \left| \frac{\langle W_i - W_j, m_i \rangle + (b_i - b_j)}{\|W_i - W_j\|} - \frac{\langle W_i - W_j, m_j \rangle + (b_i - b_j)}{\|W_i - W_j\|} \right| &= \left| \frac{\langle W_i - W_j, m_i \rangle + (b_i - b_j)}{\|W_i - W_j\|} \right| + \\ &\quad \left| \frac{\langle W_i - W_j, m_j \rangle + (b_i - b_j)}{\|W_i - W_j\|} \right|. \end{aligned}$$

Consequently,

$$\begin{aligned} \|m_i - m_j\| &\geq \left| \frac{\langle W_i - W_j, m_i \rangle + (b_i - b_j)}{\|W_i - W_j\|} \right| + \left| \frac{\langle W_i - W_j, m_j \rangle + (b_i - b_j)}{\|W_i - W_j\|} \right| \\ &= d(m_i, \mathcal{P}_{ij}) + d(m_j, \mathcal{P}_{ij}) \geq 2\delta_d. \end{aligned} \quad \blacksquare$$

So, $\|p - q\| \geq \|m_j - m_j\| - 2\delta_v \geq 2\delta_d - 2\delta_v$. With $\delta_d > 2\delta_v$, we have $\|p - q\| > 2\delta_v$. So, $\|p - q\| > \|q_1 - q_2\|$.

Appendix B. Proof of Gradients in Proposition 4.3.

Proof. If $\mathcal{L}_{\text{margin}} = 0$, then the gradient w.r.t. θ is 0, hence proposition is proved. Let us now consider the case where $\mathcal{L}_{\text{margin}} > 0$ is still larger than 0. We can easily see that

$$\nabla_{\theta} \mathcal{L}_{\text{margin}} = \text{sign}((m_c)_i - (m_c)_c) \cdot \nabla_{\theta} d(m_c, \mathcal{P}_{cj}).$$

Hence, if we show $\nabla_{\theta} d(m_c^{\text{current}}, \mathcal{P}_{ci}) = (1 - \gamma) \cdot \nabla_{\theta} d(m_c^{\text{moment}}, \mathcal{P}_{ci})$, the proposition is proved. First, we recall that for two differentiable functions: $g_1 : \mathbb{R}^{d_1} \mapsto \mathbb{R}^{d_2}$ and $g_2 : \mathbb{R}^{d_2} \mapsto \mathbb{R}^{d_3}$, and if g denotes the composed function $g := g_2 \circ g_1$, then for $x \in \mathbb{R}^{d_1}$ we have the following chain rule for computing the Jacobian matrix:

$$J_g(x) = J_{g_2}(g_1(x)) \times J_{g_1}(x).$$

In the case where $d_3 = 1$, then we have:

$$\nabla_x g = J_g(x)^T = J_{g_1}^T(x) \times J_{g_2}^T(g_1(x)) = J_{g_1}^T(x) \times \nabla_{g_1(x)} g_2.$$

Now, recall that $d(m_c, \mathcal{P}_{ci}) = \frac{|\langle W_c - W_i, m_c \rangle + (b_c - b_i)|}{\|W_c - W_i\|}$. For sake of brevity, we consider the case where $\langle W_c - W_i, m_c \rangle + (b_c - b_i) \geq 0$ and the argument is the same for the case $\langle W_c - W_i, m_c \rangle + (b_c - b_i) < 0$. We have, $d(m_c, \mathcal{P}_{ci}) = \frac{\langle W_c - W_i, m_c \rangle + (b_c - b_i)}{\|W_c - W_i\|}$. Using the chain rule from Eq. (11) with $g_2(\cdot) = \frac{|\langle W_c - W_i, \cdot \rangle + (b_c - b_i)|}{\|W_c - W_i\|}$, we get:

$$\nabla_{\theta} d(m_c^{\text{current}}, \mathcal{P}_{ci}) = J_{m_c}^T(\theta) \times \nabla_{m_c} g_2.$$

On the one hand, we can easily show that $\nabla_{m_c} g_2$ is independent of m_c and equals to $\frac{W_c - W_i}{\|W_c - W_i\|}$. So,

$$\nabla_{\theta} d(m_c, \mathcal{P}_{ci}) = J_{m_c}^T(\theta) \times \frac{W_c - W_i}{\|W_c - W_i\|}.$$

On the other hand, we have that $m_c^{\text{moment}} = \gamma \cdot m_i^{t-1} + (1 - \gamma) \cdot m_c^{\text{current}}$. Consequently,

$$J_{m_c}^T(\theta) = (1 - \gamma) \cdot J_{m_c^{\text{current}}}^T(\theta).$$

Hence, $\nabla_{\theta} d(m_c^{\text{moment}}, \mathcal{P}_{ci}) = (1 - \gamma) \cdot \nabla_{\theta} d(m_c^{\text{current}}, \mathcal{P}_{ci})$. So, \blacksquare

$$\nabla_{\theta} \mathcal{L}_{\text{margin}}^{\text{moment}} = (1 - \gamma) \cdot \nabla_{\theta} \mathcal{L}_{\text{margin}}^{\text{naive}}.$$

Appendix C. Proof of Proposition 4.4.

Recall that we work in the feature space where each point is denoted by q . Each q itself is the output of its prior layer. As assumed in the theorem, this is a convolutional layer or fully connected layer, with or without a non-linearity $ReLU$. Convolutional or fully-connected layer can be written in a general matrix-operation form as,

$$q = \begin{cases} W^- q^- + b^-, & \text{if no non-linearity.} \\ \text{ReLU}(W^- q^- + b^-), & \text{if ReLU.} \end{cases}.$$

Here, W^- and b^- are parameters of the prior layer, q^- is the input of this layer. We denote this layer by $h_{(W^-, b^-)}$. We recall that $\text{ReLU}(a) = \max(0, a)$, $\forall a \in \mathbb{R}$. When $ReLU$ is applied to a vector, we understand that $ReLU$ is applied to each element of the vector.

Remark C.1. It is obvious that $h_{\alpha(W^-, b^-)}(q^-) = \alpha h_{(W^-, b^-)}(q^-)$, $\forall \alpha \in \mathbb{R}$.

We also recall that the softmax layer has parameters (W, b) (see Eq. 3.1). For ease of notation, we refer to (W^-, b^-, b) as a flattened column-vector concatenating W^- , b^- and b . Furthermore, we denote $\Theta = \begin{pmatrix} \Theta_I \\ (W^-, b^-, b) \end{pmatrix}$, i.e., Θ_I is the vector containing all the parameters of \mathcal{N} except (W^-, b^-, b) . For an $\alpha > 0$, we define \mathcal{T}_α as

$$\mathcal{T}_\alpha : \begin{pmatrix} \Theta_I \\ (W^-, b^-, b) \end{pmatrix} \mapsto \begin{pmatrix} \Theta_I \\ \alpha(W^-, b^-, b) \end{pmatrix} := \begin{pmatrix} \tilde{\Theta}_I \\ (\tilde{W}^-, \tilde{b}^-, \tilde{b}) \end{pmatrix}.$$

In words, by applying \mathcal{T}_α on Θ , (W^-, b^-, b) is multiplied by α , that is to say $(\tilde{W}^-, \tilde{b}^-, \tilde{b}) = \alpha(W^-, b^-, b)$, and other parameters of Θ stay unchanged ($\tilde{\Theta}_I = \Theta_I$).

1. First, we prove that after applying \mathcal{T}_α , the predictions of model do not change. Consider an arbitrary input. By Remark C.1, we know that q is transformed into $\tilde{q} = \alpha q$. Moreover, from Eq. (3.1), we have

$$\tilde{z} = W\tilde{q} + \tilde{b} = \tilde{z} = W\alpha q + \alpha b = \alpha(Wq + b) = \alpha z.$$

Now, by Remark 3.1, the outputs of the new model and the old model are $\arg \max_i \alpha z_i$ and $\arg \max_i z_i$, respectively. As $\alpha > 0$, $\arg \max_i \alpha z_i = \arg \max_i z_i$. So, the new model has exactly the same prediction as the old one.

2. Now, let us consider the class margin. Recall that the distance from q to the decision boundary \mathcal{P}_{ij} (between class i and j) is $d(q, \mathcal{P}_{ij}) = \frac{|\langle W_i - W_j, q \rangle + (b_i - b_j)|}{\|W_i - W_j\|}$. So, the distance after the transformation is

$$\begin{aligned} d(\tilde{q}, \tilde{\mathcal{P}}_{ij}) &= \frac{|\langle W_i - W_j, \tilde{q} \rangle + (\tilde{b}_i - \tilde{b}_j)|}{\|W_i - W_j\|} \quad (\text{as } W \text{ stays unchanged}) \\ &= \frac{|\langle W_i - W_j, \alpha q \rangle + \alpha(b_i - b_j)|}{\|W_i - W_j\|} \\ &= \alpha \times \frac{|\langle W_i - W_j, q \rangle + (b_i - b_j)|}{\|W_i - W_j\|} = \alpha d(q, \mathcal{P}_{ij}). \end{aligned}$$

So, the distance of q to an arbitrary decision boundary is multiplied by α . As we consider an arbitrary input, by the definition of class margin, the class margin of all classes is multiplied by α .

3. Now, let us consider the class dispersion. Let consider two arbitrary points $q_1, q_2 \in \mathcal{F}$. The (euclidean) distance between these 2 points is $\|q_1 - q_2\|$. By Remark C.1, we know that q_1 and q_2 are turned into $\tilde{q}_1 := \alpha q_1$ and $\tilde{q}_2 := \alpha q_2$, respectively. Hence, the distance between these 2 points is now $\|\tilde{q}_1 - \tilde{q}_2\| = \alpha \|q_1 - q_2\|$. So, the distance between q_1 and q_2 is multiplied by α . As we chose 2 arbitrary points, this holds for any 2 points. By the definition of class dispersion, it is obvious that the class dispersion of any class is multiplied by α as well.

4. Prove that $\mathcal{T}_\alpha(\Theta) - \Theta = (\alpha - 1)u$, where u is a vector depending only on Θ . By definition of \mathcal{T}_α , we have that

$$\begin{aligned} \mathcal{T}_\alpha(\Theta) - \Theta &= \begin{pmatrix} \Theta_I \\ \alpha(W^-, b^-, b) \end{pmatrix} - \begin{pmatrix} \Theta_I \\ (W^-, b^-, b) \end{pmatrix} \\ &= \begin{pmatrix} \mathbf{0} \\ (\alpha - 1)(W^-, b^-, b) \end{pmatrix} = (\alpha - 1) \begin{pmatrix} \mathbf{0} \\ (W^-, b^-, b) \end{pmatrix}. \end{aligned}$$

So, we have that $\mathcal{T}_\alpha(\Theta) - \Theta = (\alpha - 1)u$, where $u = \begin{pmatrix} \mathbf{0} \\ (W^-, b^-, b) \end{pmatrix}$, depending only on Θ .

Appendix D. Proofs of generalization errors. In this section, we provide the complete proofs concerning the generalization errors discussed in Section 5. Our proofs are inspired by the methodology developed in [13]. To begin with, we introduce some notations and results given in [13].

Definition D.1 (Empirical Rademacher complexity, p. 30 in [13]). Let H be a family of functions mapping from \mathcal{Z} to $[a, b]$ and $S = (z_1, \dots, z_N)$ a fixed sample of size N with elements in \mathcal{Z} . Then, the empirical Rademacher complexity of H with respect to the sample S is defined as:

$$(D.1) \quad \widehat{\mathcal{R}}_S(H) = \mathbb{E}_\sigma \left[\sup_{h \in H} \frac{1}{N} \sum_{i=1}^N \sigma_i h(z_i) \right],$$

where $\sigma = (\sigma_1, \dots, \sigma_N)$, with σ_i 's independent uniform random variables taking values in $\{-1, +1\}$. The random variables σ_i are called Rademacher variables.

Theorem D.2 (Theorem 3.3, p. 31 in [13]). Let \mathcal{G} be a family of functions mapping from \mathbb{Z} to $[0, 1]$. Then, for any $\delta > 0$, with probability at least $1 - \delta$ over the draw of an i.i.d. sample S of size N , the following holds for all $g \in \mathcal{G}$:

$$\mathbb{E}[g(Z)] \leq \frac{1}{N} \sum_{i=1}^N g(z_i) + 2\widehat{\mathcal{R}}_S(\mathcal{G}) + 3\sqrt{\frac{\log \frac{2}{\delta}}{2N}}.$$

Lemma D.3 (Talagrand's lemma, p.93 in [13]). Let $\Phi : \mathbb{R} \mapsto \mathbb{R}$ be an l -Lipschitz ($l > 0$). Then, for any hypothesis set H of real-valued functions, the following inequality holds:

$$\widehat{\mathcal{R}}_S(\Phi \circ H) \leq l\widehat{\mathcal{R}}_S(H).$$

Theorem D.4 (Margin bound for binary classification, p.94 in [13]). *Let H be a set of real-valued functions and let P_X be the distribution over the input space \mathcal{X} . Fix $\rho > 0$, then, for any $\delta > 0$, with probability at least $1 - \delta$ over a sample S of size N drawn according to P_X , the following holds for all $h \in H$:*

$$(D.2) \quad R(h) \leq \widehat{R}_{S,\rho}(h) + \frac{2}{\rho} \widehat{\mathcal{R}}_S(H) + 3\sqrt{\frac{\log \frac{2}{\delta}}{2N}},$$

where $R(h) = \mathbb{E}[1_{Yh(X) < 0}]$ (generalization error), $\widehat{R}_{S,\rho}(h) = \frac{1}{N} \sum_{i=1}^N \Phi_\rho(y_i h(x_i))$ is the empirical margin loss on S of size N and $\widehat{\mathcal{R}}_S(H)$ is the empirical Rademacher complexity of H with respect to the sample S .

Using Theorem D.2 and Lemma D.3, we can derive a theorem similar to Theorem D.4 but without label as follow:

Theorem D.5. *Let H be a set of real-valued functions and let P_X be the distribution over the input space \mathcal{X} . Fix $\rho > 0$, then, for any $\delta > 0$, with probability at least $1 - \delta$ over a sample S of size N drawn according to P_X , the following holds for all $h \in H$:*

$$(D.3) \quad R(h) \leq \widehat{R}_{S,\rho}(h) + \frac{2}{\rho} \widehat{\mathcal{R}}_S(H) + 3\sqrt{\frac{\log \frac{2}{\delta}}{2N}},$$

where $R(h) = \mathbb{E}[1_{\{h(X) < 0\}}]$ (generalization error), $\widehat{R}_{S,\rho}(h) = \frac{1}{N} \sum_{i=1}^N \Phi_\rho(h(x_i))$ is the empirical margin loss on S of size N and $\widehat{\mathcal{R}}_S(H)$ is the empirical Rademacher complexity of H with respect to the sample S .

Proof. Let $\mathcal{G} = \{\Phi_\rho \circ h : h \in H\}$. By theorem D.2, for all $g \in \mathcal{G}$,

$$\mathbb{E}[g(X)] \leq \frac{1}{N} \sum_{i=1}^N g(x_i) + 2\widehat{\mathcal{R}}_S(\mathcal{G}) + 3\sqrt{\frac{\log \frac{2}{\delta}}{2N}},$$

and consequently, for all $h \in H$,

$$\mathbb{E}[\Phi_\rho(h(X))] \leq \frac{1}{N} \sum_{i=1}^N \Phi_\rho(h(x_i)) + 2\widehat{\mathcal{R}}_S(\Phi_\rho \circ H) + 3\sqrt{\frac{\log \frac{2}{\delta}}{2N}}.$$

Since $1_{\{u \leq 0\}} \leq \Phi_\rho(u)$, we have $R(h) = \mathbb{E}[1_{\{h(X) < 0\}}] \leq \mathbb{E}[\Phi_\rho(h(X))]$, so

$$R(h) \leq \widehat{R}_{S,\rho}(h) + 2\widehat{\mathcal{R}}_S(\Phi_\rho \circ H) + 3\sqrt{\frac{\log \frac{2}{\delta}}{2N}}.$$

On the other hand, since Φ_ρ is $1/\rho$ -Lipschitz, by lemma D.3, we have $\widehat{\mathcal{R}}_S(\Phi_\rho \circ H) \leq \frac{1}{\rho} \widehat{\mathcal{R}}_S(H)$.

So, $R(h) \leq \widehat{R}_{S,\rho}(h) + \frac{2}{\rho} \widehat{\mathcal{R}}_S(H) + 3\sqrt{\frac{\log \frac{2}{\delta}}{2N}}$. ■

With all these notions and theorems, we are well-equipped to prove theorems 5.2 and 5.3.

D.1. Proof of theorem 5.2. By using Theorem D.4, to prove Theorem 5.2, it suffices to prove the following result:

Theorem D.6. *Each of the following hold:*

1. *Case where $f \in \mathcal{G}_1$ is fixed. The empirical Rademacher complexity of H_f can be bounded as follows:*

$$\widehat{\mathcal{R}}_S(H_f) \leq \frac{\Gamma \sqrt{(r+R)^2 + 1}}{\sqrt{N}}.$$

2. *Case where $f \in \mathcal{G}_1$ is not fixed. The empirical Rademacher complexity of H_1 can be bounded as follows:*

$$\widehat{\mathcal{R}}_S(H_1) \leq \Gamma \sqrt{(r+R)^2 + 1}.$$

Proof. Let $\sigma = (\sigma_1, \dots, \sigma_N)$, with σ_i 's independent uniform random variables taking values in $\{-1, +1\}$. Now we calculate the Rademacher complexity.

1. Case where $f \in \mathcal{G}_1$ is fixed.

$$\begin{aligned} & \widehat{\mathcal{R}}_S(H_f) \\ &= \mathbb{E}_\sigma \left[\sup_{\|w'\| \leq \Gamma} \frac{1}{N} \sum_{i=1}^N \sigma_i (\langle f(x_i), w \rangle + b) \right] \quad (\text{where } w' := (w, b)) \\ &= \mathbb{E}_\sigma \left[\sup_{\|w'\| \leq \Gamma} \frac{1}{N} \sum_{i=1}^N \sigma_i (\langle (f(x_i), 1), (w, b) \rangle) \right] = \mathbb{E}_\sigma \left[\sup_{\|w'\| \leq \Gamma} \frac{1}{N} \sum_{i=1}^N \sigma_i (\langle (f(x_i), 1), w' \rangle) \right] \\ &= \frac{1}{N} \mathbb{E}_\sigma \left[\sup_{\|w'\| \leq \Gamma} \langle w', \sum_{i=1}^N \sigma_i (f(x_i), 1) \rangle \right] \leq \frac{1}{N} \mathbb{E}_\sigma \left[\sup_{\|w'\| \leq \Gamma} \|w'\| \times \left\| \sum_{i=1}^N \sigma_i (f(x_i), 1) \right\| \right] \\ &\leq \frac{\Gamma}{N} \mathbb{E}_\sigma \left[\left\| \sum_{i=1}^N \sigma_i (f(x_i), 1) \right\| \right] \leq \frac{\Gamma}{N} \left(\mathbb{E}_\sigma \left[\left\| \sum_{i=1}^N \sigma_i (f(x_i), 1) \right\|^2 \right] \right)^{\frac{1}{2}} \quad (\text{Jensen's inequality}) \\ &= \frac{\Gamma}{N} \left(\mathbb{E}_\sigma \left[\sum_{i,j=1}^N \sigma_i \sigma_j \langle (f(x_i), 1), (f(x_j), 1) \rangle \right] \right)^{\frac{1}{2}} \\ &= \frac{\Gamma}{N} \left(\mathbb{E}_\sigma \left[\sum_{i=1}^N \|(f(x_i), 1)\|^2 \right] \right)^{\frac{1}{2}} \quad (\mathbb{E}_\sigma[\sigma_i \sigma_j] = 0 \text{ if } i \neq j \text{ and } 1 \text{ otherwise}) \\ &= \frac{\Gamma}{N} \left(\mathbb{E}_\sigma \left[\sum_{i=1}^N (\|f(x_i)\|^2 + 1) \right] \right)^{\frac{1}{2}} = \frac{\Gamma}{N} \left(N + \mathbb{E}_\sigma \left[\sum_{i=1}^N \|f(x_i)\|^2 \right] \right)^{\frac{1}{2}}. \end{aligned}$$

Now, notice that by triangle inequality, we have $\|f(x_i)\| \leq \|f(x_i) - m(q(i))\| + \|m(q(i))\|$, where $m(q(i)) \in \{m_1, m_2\}$ is the center of the hypersphere of radius r containing q_i (recall that $q_i = f(x_i)$). This means that $\|f(x_i) - m(q(i))\| \leq r$ and $\|m(q(i))\| \leq R$. So, $\|f(x_i)\| \leq R + r$. Thus, $\widehat{\mathcal{R}}_S(H_f) \leq \frac{\Gamma}{N} \left(N + \mathbb{E}_\sigma \left[\sum_{i=1}^N (R+r)^2 \right] \right)^{\frac{1}{2}} = \frac{\Gamma}{N} \sqrt{N + N(R+r)^2} = \frac{\Gamma \sqrt{(r+R)^2 + 1}}{\sqrt{N}}.$

2. Case where $f \in \mathcal{G}_1$ is not fixed.

$$\begin{aligned}
\widehat{\mathcal{R}}_S(H) &= \mathbb{E}_\sigma \left[\sup_{\|w'\| \leq \Gamma, f \in \mathcal{G}_1} \frac{1}{N} \sum_{i=1}^N \sigma_i(\langle f(x_i), w' \rangle + b) \right] \\
&= \frac{1}{N} \mathbb{E}_\sigma \left[\sup_{\|w'\| \leq \Gamma, f \in \mathcal{G}_1} \sum_{i=1}^N \sigma_i(\langle (f(x_i), 1), w' \rangle) \right] \\
&= \frac{1}{N} \mathbb{E}_\sigma \left[\sup_{\|w'\| \leq \Gamma, f \in \mathcal{G}_1} \langle w, \sum_{i=1}^N \sigma_i(f(x_i), 1) \rangle \right] \\
&\leq \frac{1}{N} \mathbb{E}_\sigma \left[\sup_{\|w'\| \leq \Gamma, f \in \mathcal{G}_1} \|w'\| \times \left\| \sum_{i=1}^N \sigma_i(f(x_i), 1) \right\| \right] \\
&\leq \frac{\Gamma}{N} \mathbb{E}_\sigma \left[\sup_{f \in \mathcal{G}_1} \left\| \sum_{i=1}^N \sigma_i(f(x_i), 1) \right\| \right] \leq \frac{\Gamma}{N} \mathbb{E}_\sigma \left[\sup_{f \in \mathcal{G}_1} \sum_{i=1}^N \|\sigma_i(f(x_i), 1)\| \right] \\
&= \frac{\Gamma}{N} \mathbb{E}_\sigma \left[\sup_{f \in \mathcal{G}_1} \sum_{i=1}^N \|(f(x_i), 1)\| \right] \leq \frac{\Gamma}{N} \mathbb{E}_\sigma \left[\sum_{i=1}^N \sup_{f \in \mathcal{G}_1} \|(f(x_i), 1)\| \right] \\
&= \frac{\Gamma}{N} \mathbb{E}_\sigma \left[\sum_{i=1}^N \sup_{f \in \mathcal{G}_1} \sqrt{\|(f(x_i))\|^2 + 1} \right] \\
&\leq \frac{\Gamma}{N} \mathbb{E}_\sigma \left[\sum_{i=1}^N \sqrt{(r+R)^2 + 1} \right] \quad (\sup_{f \in \mathcal{G}_1} \|f(x_i)\| \leq r+R \text{ similarly to Case 1}) \\
&= \frac{\Gamma}{N} \times N \sqrt{(r+R)^2 + 1} = \Gamma \sqrt{(r+R)^2 + 1}. \quad \blacksquare
\end{aligned}$$

D.2. Proof of Theorem 5.3. By using Theorem D.5, to prove Theorem 5.3, it suffices to prove the following result:

Theorem D.7. *The empirical Rademacher complexity of H_2 can be bounded as follows:*

$$(D.4) \quad \widehat{\mathcal{R}}_S(H_2) \leq \Lambda^2 + 2R\Lambda + \frac{R^2}{\sqrt{N}}.$$

Proof. Let $\mathcal{G}_2 = \{f : \|\sup_{x \in \mathcal{X}} f(x)\| \leq \Lambda\}$. Let $\sigma = (\sigma_1, \dots, \sigma_N)$, with σ_i 's independent uniform random variables taking values in $\{-1, +1\}$. By definition of the empirical Rademacher complexity, we have:

$$\begin{aligned}
& \widehat{\mathcal{R}}_S(H_2) \\
&= \mathbb{E}_\sigma \left[\sup_{\|m\| \leq R, f \in \mathcal{G}_2} \frac{1}{N} \sum_{i=1}^N \sigma_i (r^2 - \|f(x_i) - m\|^2) \right] \\
&= \frac{1}{N} \mathbb{E}_\sigma \left[\sum_{i=1}^N \sigma_i r^2 + \sup_{\|m\| \leq R, f \in \mathcal{G}_2} \sum_{i=1}^N -\sigma_i \|f(x_i) - m\|^2 \right] \\
&= \frac{1}{N} \mathbb{E}_\sigma \left[\sup_{\|m\| \leq R, f \in \mathcal{G}_2} \sum_{i=1}^N -\sigma_i \|f(x_i) - m\|^2 \right] \quad \left(\text{as } \mathbb{E}_\sigma \left[\sum_{i=1}^N \sigma_i r^2 \right] = r^2 \sum_{i=1}^N \mathbb{E}_\sigma[\sigma_i] = 0 \right) \\
&= \frac{1}{N} \mathbb{E}_\sigma \left[\sup_{\|m\| \leq R, f \in \mathcal{G}_2} \sum_{i=1}^N (-\sigma_i \|f(x_i)\|^2 - \sigma_i \|m\|^2 + 2\sigma_i \langle f(x_i), m \rangle) \right] \\
&\leq \frac{1}{N} \mathbb{E}_\sigma \left[\sup_{f \in \mathcal{G}_2} \sum_{i=1}^N -\sigma_i \|f(x_i)\|^2 + \sup_{\|m\| \leq R} \sum_{i=1}^N -\sigma_i \|m\|^2 + \sup_{\|m\| \leq R, f \in \mathcal{G}_2} \sum_{i=1}^N 2\sigma_i \langle f(x_i), m \rangle \right].
\end{aligned}$$

Considering each term inside the expectation operation, we get,

$$\begin{aligned}
\mathbb{E}_\sigma \left[\sup_{f \in \mathcal{G}_2} \sum_{i=1}^N -\sigma_i \|f(x_i)\|^2 \right] &\leq \mathbb{E}_\sigma \left[\sup_{f \in \mathcal{G}_2} \left| \sum_{i=1}^N -\sigma_i \|f(x_i)\|^2 \right| \right] \leq \mathbb{E}_\sigma \left[\sup_{f \in \mathcal{G}_2} \sum_{i=1}^N |\sigma_i \|f(x_i)\|^2| \right] \\
&= \mathbb{E}_\sigma \left[\sup_{f \in \mathcal{G}_2} \sum_{i=1}^N \|f(x_i)\|^2 \right] \leq \mathbb{E}_\sigma \left[\sum_{i=1}^N \Lambda^2 \right] = N\Lambda^2.
\end{aligned}$$

Consider now the second term. We have,

$$\begin{aligned}
\mathbb{E}_\sigma \left[\sup_{\|m\| \leq R} \sum_{i=1}^N -\sigma_i \|m\|^2 \right] &\leq \mathbb{E}_\sigma \left[\sup_{\|m\| \leq R} \left| \sum_{i=1}^N -\sigma_i \|m\|^2 \right| \right] = \mathbb{E}_\sigma \left[\sup_{\|m\| \leq R} \|m\|^2 \left| \sum_{i=1}^N \sigma_i \right| \right] \\
&\leq R^2 \mathbb{E}_\sigma \left[\left| \sum_{i=1}^N \sigma_i \right| \right] \leq R^2 \left(\mathbb{E}_\sigma \left[\left| \sum_{i=1}^N \sigma_i \right|^2 \right] \right)^{\frac{1}{2}} \\
&= R^2 \left(\mathbb{E}_\sigma \left[\sum_{i,j=1}^N \sigma_i \sigma_j \right] \right)^{\frac{1}{2}} \\
&= R^2 \left(\mathbb{E}_\sigma \left[\sum_{i=1}^N \sigma_i^2 \right] \right)^{\frac{1}{2}} \quad (\text{as } \mathbb{E}_\sigma[\sigma_i \sigma_j] = 0 \text{ if } i \neq j \text{ and } 1 \text{ otherwise}) \\
&= R^2 \sqrt{N}.
\end{aligned}$$

Consider now the final term inside the expectation operation.

$$\begin{aligned}
\mathbb{E}_\sigma \left[\sup_{\|m\| \leq R, f \in \mathcal{G}_2} \sum_{i=1}^N 2\sigma_i \langle f(x_i), m \rangle \right] &\leq \mathbb{E}_\sigma \left[\sup_{\|m\| \leq R, f \in \mathcal{G}_2} \left| \sum_{i=1}^N 2\sigma_i \langle f(x_i), m \rangle \right| \right] \\
&\leq \mathbb{E}_\sigma \left[\sup_{\|m\| \leq R, f \in \mathcal{G}_2} \left| \sum_{i=1}^N 2\sigma_i \|f(x_i)\| \cdot \|m\| \right| \right] \\
&\leq \mathbb{E}_\sigma \left[2R \sup_{f \in \mathcal{G}_2} \sum_{i=1}^N |\sigma_i| \cdot \|f(x_i)\| \right] \\
&= \mathbb{E}_\sigma \left[2R \sup_{f \in \mathcal{G}_2} \sum_{i=1}^N \|f(x_i)\| \right] \leq \mathbb{E}_\sigma \left[2R \sum_{i=1}^N \Lambda \right] = 2NR\Lambda .
\end{aligned}$$

Hence, $\widehat{\mathcal{R}}_S(H_2) \leq \frac{1}{N}(\Lambda^2 N + R^2 \sqrt{N} + 2NR\Lambda) = \Lambda^2 + 2R\Lambda + \frac{R^2}{\sqrt{N}}$. ■

Appendix E. Proof of Theorem 6.3. We first recall some definitions and lemmas needed in the proof.

Definition E.1 (Total variation distance). Let \mathcal{D}_1 and \mathcal{D}_2 be probability measures on a measurable space Ω . The total variation (TV) distance between \mathcal{D}_1 and \mathcal{D}_2 is defined as

$$d_{TV}(\mathcal{D}_1, \mathcal{D}_2) = \sup_{S \subseteq \Omega} |\mathcal{D}_1(S) - \mathcal{D}_2(S)| .$$

Lemma E.2 (Pinsker's inequality). For every $\mathcal{D}_1, \mathcal{D}_2$ on Ω ,

$$d_{TV}(\mathcal{D}_1, \mathcal{D}_2) \leq \sqrt{\frac{1}{2} D_{KL}(\mathcal{D}_1 \| \mathcal{D}_2)} .$$

Lemma E.3 (Relation between JSD and mutual information). Let B be the equiprobable binary r.v. taking value in $\{0, 1\}$. Given two distributions \mathcal{D}_1 and \mathcal{D}_2 , let $X_1 \sim \mathcal{D}_1$ let $X_2 \sim \mathcal{D}_2$. Assume that X_1 and X_2 are independent of B , let $X = BX_1 + (1 - B)X_2$. Then, we have

$$(E.1) \quad D_{JS}(\mathcal{D}_1 \| \mathcal{D}_2) = I(X, B) ,$$

where $I(X, B)$ is the mutual information of X and B (see [2]).

Remark. We see that we choose the value of X according to \mathcal{D}_1 if $B = 0$ and according to \mathcal{D}_2 if $B = 1$. That is, $\mathcal{D}(X|B = 0) = \mathcal{D}_1$ and $\mathcal{D}(X|B = 1) = \mathcal{D}_2$. Hence, B can be considered as ‘‘flipping variable’’. Moreover, notice that in Eq. (E.1), the entropy (used in the mutual information) is with respect to a reference measure and that implicitly \mathcal{D}_1 and \mathcal{D}_2 are absolutely continuous with respect to this reference measure.

Now, we are ready for the proof.

Proof. We consider any class pair $(y \neq y') \in \mathcal{Y}^2$. Let us first consider the conditional distributions on \mathcal{F} . We have that

$$\begin{aligned} d_{TV} \left(\mathcal{D}_{Q|y}, \frac{\mathcal{D}_{Q|y} + \mathcal{D}_{Q|y'}}{2} \right) &= \sup_{S \subseteq \mathcal{F}} \left| \mathcal{D}_{Q|y}(S) - \frac{\mathcal{D}_{Q|y}(S) + \mathcal{D}_{Q|y'}(S)}{2} \right| \\ &= \sup_{S \subseteq \mathcal{F}} \left| \frac{\mathcal{D}_{Q|y}(S) - \mathcal{D}_{Q|y'}(S)}{2} \right|. \end{aligned}$$

We consider $S = \mathcal{S}(m_y, \delta_v)$, the hyper-sphere of radius δ_v centered at m_y . Recall that we have assumption $\mathcal{D}_{Q|y}(\mathcal{S}(m_y, \delta_v)) \geq \tau$, $\forall y \in \mathcal{Y}$ ($1/2 \leq \tau \leq 1$). Hence, we have $\mathcal{D}_{Q|y}(S) \geq \tau$.

Moreover, as the hyper-spheres of each class are disjoint, $S = \mathcal{S}(m_y, \delta_v) \subseteq \mathcal{F} \setminus \mathcal{S}(m_{y'}, \delta_v)$. So, $\mathcal{D}_{Q|y'}(S) \leq \mathcal{D}_{Q|y'}(\mathcal{F} \setminus \mathcal{S}(m_{y'}, \delta_v)) = 1 - \mathcal{D}_{Q|y'}(\mathcal{S}(m_{y'}, \delta_v)) \leq 1 - \tau$.

Therefore, we have that $\mathcal{D}_y(S) - \mathcal{D}_{y'}(S) \geq \tau - (1 - \tau) = 2\tau - 1$. Note that this term is positive as $\tau \geq 1/2$. Hence, $|\mathcal{D}_y(S) - \mathcal{D}_{y'}(S)| = \mathcal{D}_y(S) - \mathcal{D}_{y'}(S) \geq 2\tau - 1$.

So, $d_{TV} \left(\mathcal{D}_{Q|y}, \frac{\mathcal{D}_{Q|y} + \mathcal{D}_{Q|y'}}{2} \right) = \sup_{S \subseteq \mathcal{F}} |\mathcal{D}_{Q|y}(S) - \mathcal{D}_{Q|y'}(S)|/2 \geq (2\tau - 1)/2$.

Using Lemma E.2, we have that

$$\frac{1}{2} D_{KL} \left(\mathcal{D}_{Q|y} \parallel \frac{\mathcal{D}_{Q|y} + \mathcal{D}_{Q|y'}}{2} \right) \geq d_{TV} \left(\mathcal{D}_{Q|y}, \frac{\mathcal{D}_{Q|y} + \mathcal{D}_{Q|y'}}{2} \right) \geq \frac{(2\tau - 1)^2}{4}.$$

As this hold for any $(y \neq y') \in \mathcal{Y}$, we also have that

$$\frac{1}{2} D_{KL} \left(\mathcal{D}_{Q|y'} \parallel \frac{\mathcal{D}_{Q|y} + \mathcal{D}_{Q|y'}}{2} \right) \geq \frac{(2\tau - 1)^2}{4}.$$

Therefore, by summing these 2 terms, using the definition of JSD, we have

$$(E.2) \quad D_{JS}(\mathcal{D}_{Q|y} \parallel \mathcal{D}_{Q|y'}) \geq \frac{(2\tau - 1)^2}{2}.$$

Let B be the equiprobable binary r.v. taking value in $\{0, 1\}$. Consider now the conditional distributions $\mathcal{D}_{Q^l|y}$ and $\mathcal{D}_{Q^l|y'}$ in the feature space \mathcal{F}^l of a layer l before the penultimate layer. Let Q_B^l be the random variable associated to a mixture distribution of $\mathcal{D}_{Q^l|y}$ and $\mathcal{D}_{Q^l|y'}$ with B as flipping variable in the way defined in Lemma E.3. So, we have

$$(E.3) \quad D_{JS}(\mathcal{D}_{Q^l|y} \parallel \mathcal{D}_{Q^l|y'}) = I(B, Q_B^l).$$

Let f_l denote the mapping representing the set of layers between layer l and the penultimate layer. So, we have that the distributions $\mathcal{D}_{Q|y}$ and $\mathcal{D}_{Q|y'}$ are induced by f_l from $\mathcal{D}_{Q^l|y}$ and $\mathcal{D}_{Q^l|y'}$, respectively. Let $Q_B = f_l(Q_B^l)$. So we have the Markovian relationship: $B \rightarrow Q_B^l \rightarrow Q_B$. The data processing inequality [2] follows that

$$(E.4) \quad I(B, Q_B^l) \geq I(B, Q_B).$$

Moreover, note that the distribution \mathcal{D}_{Q_B} is induced by f_l from $\mathcal{D}_{Q_B^l}$. Given $B = 0$, $\mathcal{D}(Q_B^l|B=0) = \mathcal{D}_{Q^l|y}$. So, the distribution $\mathcal{D}(Q_B|B=0)$ is induced from $\mathcal{D}_{Q^l|y}$ by f_l . That

is, $\mathcal{D}(Q_B|B=0) = \mathcal{D}_{Q|y}$. Similarly, we also have $\mathcal{D}(Q_B|B=1) = \mathcal{D}_{Q|y'}$. Hence, by Lemma E.3, we have

$$(E.5) \quad D_{JS}(\mathcal{D}_{Q|y} \parallel \mathcal{D}_{Q|y'}) = I(B, Q_B) .$$

From (E.3), (E.4) and (E.5), we have $D_{JS}(\mathcal{D}_{Q^i|y} \parallel \mathcal{D}_{Q^i|y'}) \geq D_{JS}(\mathcal{D}_{Q|y} \parallel \mathcal{D}_{Q|y'})$. Combining with (E.2), we have that

$$D_{JS}(\mathcal{D}_{Q^i|y} \parallel \mathcal{D}_{Q^i|y'}) \geq \frac{(2\tau - 1)^2}{2} .$$

This completes the proof. ■

Appendix F. Experiment details. In this section, we provide the details for conducting our experiments. All of our experiments are performed using *Pytorch*.

F.1. Training ResNet18. We intentionally aimed to keep a very minimal setup. Thus, we use the same training scheme for all the experiments with ResNet18, with softmax loss and our loss, on both CIFAR10 and SVHN (including the ablation study). We use SGD optimizer with nesterov momentum, with initial learning rate of 10^{-3} (decayed by factor of 5 at epochs 60, 120 and 160), momentum 0.9, weight decay $5 \cdot 10^{-4}$. Model is trained for 200 epochs.

We use non-linearity *ReLU* for the last convolutional layer of ResNet18. Then, we add a fully-connected layer with output dimension of 30 prior to the final softmax layer (with output dimension of 10 for 10 classes). As presented, our loss function is applied on the penultimate layer, meaning the layer with output dimension of 30.

For the training sets of CIFAR10 and SVHN, we apply data augmentation techniques including Random Cropping (padding=4) and Random Horizontal Flipping.

F.2. Training EfficientNet-b0 and MobileNetV3 on RSCD dataset. We use models pre-trained on *ImageNet* as initialization. During training, we apply data augmentation techniques including Random Perspective and Random Horizontal Flipping. We use Adam optimizer with learning rate 10^{-4} . We train models for 20 epochs and keep the best models based on the validation accuracy.